USF Tampa Graduate Theses and Dissertations   USF Graduate Theses and Dissertations

7-14-2010

Investigation of Buildup Dose for Therapeutic Intensity Modulated Photon Beams in Radiation Therapy

Khosrow Javedan
University of South Florida

Follow this and additional works at: https://digitalcommons.usf.edu/etd

Part of the American Studies Commons, Biomedical Engineering and Bioengineering Commons, and the Chemical Engineering Commons

Investigation of Buildup Dose for Therapeutic Intensity Modulated

Photon Beams in Radiation Therapy

by

Khosrow Javedan

A dissertation submitted in partial fulfillment
of the requirements for the degree of
Doctor of Philosophy
Department of Chemical and Biomedical Engineering
College of Engineering
University of South Florida

Co-Major Professor: William E. Lee III, Ph.D.
Co-Major Professor: Harvey M. Greenberg, M.D.
Geoffrey Zhang, Ph.D.
Kenneth M. Forster, Ph.D.
Kent H. Larsen, Ph.D.
Paris H. Wiley, Ph.D.

Date of Approval:
July 14, 2010

DEDICATION

To my family.

ACKNOWLEDGEMENTS

TABLE OF CONTENTS

LIST OF TABLES

LIST OF FIGURES

Investigation of Buildup Dose for Therapeutic Intensity Modulated

Photon Beams in Radiation Therapy

Khosrow Javedan

ABSTRACT

Buildup dose of Mega Voltage (MV) photon beams can be a limiting factor in intensity-modulated radiation therapy (IMRT) treatments. Excessive doses can cause patient discomfort and treatment interruptions, while underdosing may lead to local failure.

Many factors which contribute to buildup dose, including the photon beam energy spectrum, scattered or contaminant radiation and their angular distribution, are not modeled well in commercial treatment planning systems. The accurate Monte Carlo method was employed in the studies to estimate the doses.

Buildup dose of 6MV photon beams was investigated for three fundamentally different IMRT modalities: between Helical TomoTherapy and traditional opposed tangential beams, solid IMRT and multileaf collimator (MLC)-based IMRT techniques. Solid IMRT, as an alternative to MLC, achieves prescription dose distribution objectives, according to our study.

Measurements and Monte Carlo calculations of buildup dose in chest wall treatment were compared between TomoTherapy IMRT and traditional tangential-beam technique. The effect of bolus in helical delivery was also investigated in this study.

In addition, measurements and Monte Carlo calculations of buildup dose in solid IMRT and MLC based IMRT treatment modalities were compared. A brass step compensator was designed and built for the solid IMRT. Matching MLC step sequences were used for the MLC IMRT.

This dissertation also presents the commissioning of a Monte Carlo code system, BEAMnrc, for a Varian Trilogy linear accelerator (LINAC) and the application in buildup dose calculation. Scattered dose components, MLC component dose and mean spectral energy for the IMRT treatment techniques were analyzed.

The agreement between measured 6MV and calculated depth dose and beam profiles was ($\pm$ 1% or $\pm$1 mm) for 10x10 and 40x40 cm^2 fields. The optimum electron beam energy and its radial distribution incident on tungsten target were found to be 6 MeV and 1 mm respectively.

The helical delivery study concluded that buildup dose is higher with TomoTherapy compared to the opposed tangential technique in chest wall treatment. The solid and MLC IMRT comparison concluded that buildup dose was up to 7% lower for solid IMRT compared to MLC IMRT due to beam hardening of brass.

CHAPTER 1 INTRODUCTION

1.1 Synopsis

Determination of buildup dose of therapeutic megavoltage photon beams has been an active area of research in radiation therapy since before the introduction of 3D conformal radiation therapy[1], a precursor to IMRT[2]. Accurate knowledge of buildup dose of IMRT is necessary, especially for IMRT cases treated with concurrent radiosentisising chemotherapy where excessive dose in the buildup region can cause skin infection and treatment interruption, and underdosing may lead to local failure. Dose in this region must accurately be known so that the calculated dose by the treatment planning system (TPS) is properly interpreted. A radiation oncologist may have to compromise a known therapeutic dose in order to limit the skin dose calculated by the treatment planning system (TPS). Historically, superficial dose is not well predicted by commercial TPS. Literature shows TPS overestimate dose in the buildup region by up to 19%. Literature also shows the expected calculation accuracy for pass fail criteria in the buildup region when commissioning the TPS is 20% of the normalization dose for open fields[3]. It is up to the individual physicist to accurately assess the shallow dose and incorporate that into evaluating the TPS dose in the buildup region.

Many factors contribute to buildup dose, including the photon beam energy spectrum, contaminant electrons and scattered particle angular distribution, and effect of immobilization devices which are not properly modeled in commercial treatment planning systems. The dosimetrical differences in buildup regions between different treatment modalities, such as helical IMRT delivery with TomoTherapy versus traditional wedge pair technique, and MLC-based versus compensator-based IMRT, cannot be accurately obtained by comparing treatment plans alone.

This dissertation work investigates the dosimetrical differences in buildup region between TomoTherapy versus conventional wedge pair technique with and without bolus, and IMRT with MLC versus solid brass compensator with measurement and Monte Carlo method. Significant work was carried out in establishing and running the Monte Carlo Code system on the Moffitt Computer Cluster and in commissioning the BEAM to perform radiation transport calculations with the same beam characteristics as the 6MV Varian Clinac 2100 beam. Use of this code was an essential part of this dissertation.

1.2 Objective of the Study

The objective of the study was to investigate the dosimetrical differences including the dose and dose gradient in the buildup region of therapeutic photon beams from 3 different IMRT modalities: TomoTherapy, compensator-based IMRT and MLC-based IMRT. The dose and relative dose distributions were measured with film, ion chamber and MOSFET detectors and calculated with Monte Carlo to verify the doses. The results of the study

were used to answer important clinical concerns related to the IMRT technique used. For example, whether chest wall treatment with TomoTherapy requires the use of bolus material, whether solid IMRT can achieve the prescription dose distribution objectives as an alternative to MLC-based IMRT, and whether buildup dose of IMRT delivery with compensator on the Varian Clinac 2100 LINAC is a concern.

The secondary objective and essential part of this dissertation was to install the EGSnrc, BEAMnrc Monte Carlo code system on the institution's computer cluster and test to ensure proper functionality of the installed code and related programs, such as DOSXYZnrc, statdose, BEAM_DP and ctcreate. The Monte Carlo BEAM was commissioned to perform radiation transport calculations with the same beam characteristics as the 6MV beam of the LINAC used.

1.3 Dissertation Outline

The European format of using peer-reviewed journal articles in compiling the bulk of this manuscript has been adopted for this dissertation. Therefore, there may be overlapping text in various chapters of this work. This was ascertained to be the most efficient arrangement in order to preserve the overall quality of this work.

Chapter 2 describes the commissioning of the Monte Carlo simulation code BEAMnrc and DOSXYZnrc for the application in the dissertation studies.

Chapter 3 discusses the skin dose differences between TomoTherapy chest wall irradiation and traditional linear-accelerator-based tangential-beam technique. Adequate treatment of the chest wall using the tangential-beam technique is reviewed. Chest wall plans that were generated using two commercial treatment planning systems which produce plans for fundamentally different dose delivery methods, along with Monte Carlo dose calculations were evaluated to determine if bolus was required for adequate skin dose from the two treatment techniques.

Chapter 4 investigates the use of solid brass modulators for intensity-modulated radiation therapy (IMRT) delivery of large targets as an alternative to step and shoot delivery with multileaf collimator (MLC)[15]. This study was conducted during the initial use of solid modulators in the department to investigate the device's ability to reproduce the planned isodose distribution for a large target which overlapped normal critical structures. An ideal modulator is one which faithfully reproduces the field's ideal intensity map as planned, both dosimetrically and spatially. The dose volume histogram (DVH) of IMRT plans with solid modulator and MLC was compared. The absolute point doses were measured with a calibrated ionization chamber. The relative dose distribution was measured with EDR2 film and a commercial diode array device to ensure the planned isodoses matched the delivered isodose distributions.

Chapter 5 investigates the dosimetrical differences in buildup region of a 6MV beam between MLC- and compensator-based IMRT with measurement and Monte Carlo method. Photon beam energy spectrum, contaminant electrons and scattered particle

angular distribution affect the buildup dose and are not properly modeled in commercial treatment planning systems. Literature suggests such systems overestimate the dose in this region. Since buildup dose near skin is not accurately predicted by commercial treatment planning systems, accurate Monte Carlo was used to calculate the near skin buildup dose at depth of 1.0-5.0 mm. Skin dose variation with SSD, field size and beam incidence angle was investigated. Component doses of contaminant photons, contaminant electrons and MLC component dose was calculated for the two IMRT delivery systems. Mean spectral energy as a function of brass modulation was calculated to show beam hardening effect responsible for enhanced skin sparing of the solid modulator.

1.4 Limitation of this Work

The Monte Carlo simulation package BEAMnrc was commissioned for the 6MV photon beam from Varian Trilogy LINAC equipped with MLC. However, Varian Trilogy machine also produces 15MV photon beams and 6 electron beams of 6 MeV to 22 MeV (commissioning these energies is left for future work). Due to simplified design of the brass step jig, we could accurately model the steps of solid modulator and dose equivalent MLC sequences to perform simulation and dose and component dose calculation in the buildup region. Clinical IMRT beams may require highly complex dose distribution in X, Y and Z direction, modulated with solid brass or MLC. The modeling of such a complex device with BEAMnrc was out of scope of this research.

CHAPTER 2 MONTE CARLO SIMULATION

2.1 Synopsis

Monte Carlo simulation is a numerical solution to a problem that is not easily solved by analytical methods. The problem models objects (i.e, high energy electron and photon radiation) that interact with other objects (i.e, matter) in a well defined environment. A solution (result of interaction based on actual radiation transport physics) is determined by repeated random sampling using computational algorithms to calculate the result.

Monte Carlo simulations are employed in many fields such as radiation physics, chemistry, space, finance, mathematics, and other disciplines that may require a quantitative solution to a problem which can be approximated by statistical sampling. Monte Carlo techniques for simulating radiation transport of electrons and photons are used extensively in the field of medical physics and radiation dosimetry[4]. Monte Carlo simulation has been found to be the most accurate technique to estimate the dose deposited in tissue based on the actual radiation transport physics[5, 6].

2.2 Monte Carlo Simulation of Megavoltage Photon Beam

Monte Carlo simulation starts as the monoenergetic electron beam with initial kinetic energy E_{ki} interacts with the nuclei of the high Z tungsten target atom mostly by the way

of Coulomb interaction. The incident electrons also scatter and lose energy through production of x-ray bremsstrahlung photons. Bremsstrahlung photons are produced at a rate expressed by the mass radiative stopping power $(dT/\rho dx)_r$, in units of MeV cm^2/g as in equation 1,

$$\left(\frac{dT}{\rho dx}\right)_r \propto \frac{Z^2}{A} \frac{1}{(m_o c^2)^2} \tag{1}$$

Z^2/A refers to the atomic number and mass number of the medium and $(m_o c^2)$ is the rest energy of the charged particle. Bremsstrahlung is produced at higher rate for the high Z target compared to low Z target due to the Z^2 dependence.

Each particle is transported and tracked as it passes through and interacts with various components in the accelerator head in its path. Such components are the primary collimator (defines radiation port), thin vaccum window (target assembly kept in vacuum), flattening filter (has cone shaped geometry, made of low-medium Z material, reduces the forward peaked photon fluence more in the center than periphery to produce flat beam), transmission chamber (monitors dose, beam flatness and symmetry), mirror (locked in place in x-ray mode to project field light on surface), secondary jaws (high Z material defines field size), MLC (high Z material shapes fields with motorized leaves) and the intervening air until it reaches the end of its history. It then either escapes the defined geometry or deposits its energy at the end of its track.

The end of each particle's track is determined by its cut off energy. Once particle energy falls below its cut off energy, the particle is no longer tracked and all of its energy is deposited at the site, notwithstanding that Compton scattering is the predominant mode of interaction for the 6MV photon beam, interacting with low Z absorbers such as the flattening filter material, muscle and water.

2.3 Materials and Methods

2.3.1 Monte Carlo Simulation of the Varian Clinac 6MV Beam

An EGSnrc[7, 8]-based Monte Carlo simulation package for clinical radiation treatment units, BEAMnrc [9], was used to precisely characterize a Varian Clinac 2100 LINAC (Varian Medical Systems, Palo Alto, CA) equipped with MLC.

The detailed drawing including the material and geometry for the accelerator head components and the distance of each component from the target was acquired from the manufacturer. The component modules (CMs) of BEAMnrc were used to precisely model the accelerator head components in the accelerator input file.

2.3.2 Component Modules of BEAMnrc

Component modules are blocks with front surface and back surface. All blocks are completely independent. Various CMs are used to model exact geometry and material of

different components in the LINAC head. Each component assumes a horizontal slab portion of the accelerator with respect to beam axis. Each specialized CM can be used more than once to model different parts of the accelerator, therefore a unique name was given to each component's CM for the simulation.

2.3.3 CMs for Varian Clinac 2100 Model

The CMs that were used to model the Varian Clinac 2100 were SLABS for target, CONS3R for primary collimator, SLABS for vacuum window, FLATFIL for flattening filter, CHAMBER for transmission monitor chamber, MIRROR for mirror, JAWS for secondary collimator jaws, SLABS for air gap, and CHAMBER as phantom for phantom defined at 100 cm SSD (source to surface distance). Phantom in BEAMnrc input file was used to simulate depth dose in water along the central-axis.

The MLC was modeled using VARMLC CM in BEAMnrc. This module models the leaves, the air gap between leaves, the leaf tongue-in-groove and the driving screws at the top and bottom of each leaf.

The accelerator model that was used to perform MC simulations is shown in Figure 1.
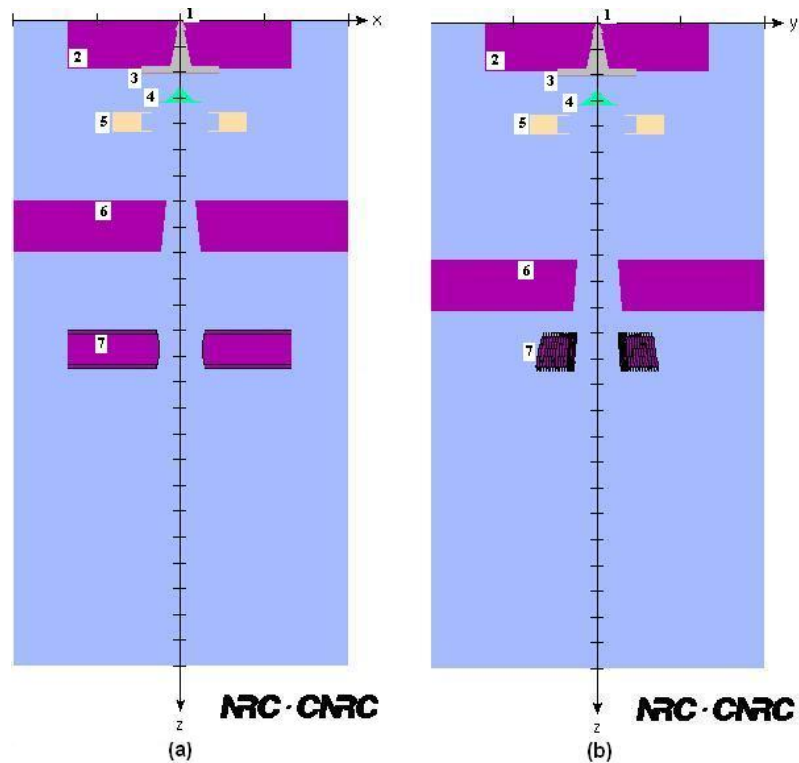
Figure 1. The accelerator model for the 6MV Varian 2100 and its component modules in (a) XZ view, and (b) YZ view. The accelerator components are the target (1), the primary collimator (2), the vacuum window (3), the flattening filter (4), the transmission chamber (5), the secondary jaws (6) and the MLC (7), as shown in the figure.

2.3.4 DOSXYZnrc

DOSXYZnrc[13] is another Monte Carlo simulation program which is used to calculate dose distribution in a simple rectilinear phantom geometry. The phantom is defined within the program by the user. For example a 40x40x40 cm^3 water phantom was defined. Also the voxel size in X, Y, and Z dimension was input and dose distribution calculation planes either parallel or normal to the beam axis were defined. Percent depth dose and beam profiles were calculated using this program.

10

2.3.5 Measured Beam Data

Beam data including the percent depth dose and beam profiles were acquired during the commissioning of the LINAC. Scanned beam data were measured with ion chamber and diode using a commercial water scanning system (Scanditronix-Welhoffer RFA 300).

2.3.6 Accelerator Simulation Parameters

Three electron beam incident energies of 5.7, 6.0 and 6.3 MeV were investigated. The calculated percentage depth dose and beam profiles were compared with the 6MV scanned beam data to determine the optimum value for the electron beam energy incident on the target.

The incident electron beam source was chosen as parallel circular beam with a uniform distribution (ISOURCC=1), as shown in Figure 2. In the accelerator input file, this source model takes four input parameters, the beam radius and the (x, y, z)-direction cosines. The x- and y-axis direction cosine was set to zero and the z-axis direction cosine was set to 1 to define the incident beam orientation parallel to the z-axis and pointing down the accelerator.
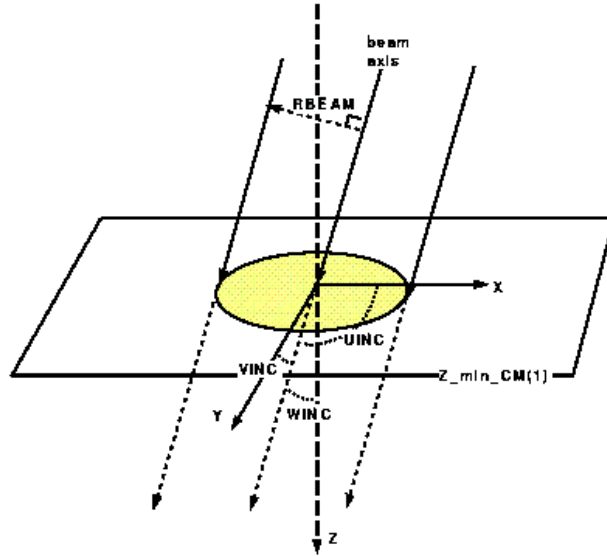
Figure 2. Source model as parallel circular beam with a uniform distribution. (ISOURC=1)[9] is shown. The beam radius and the x,y,z -direction cosines are the 4 parameters used to define the source. The parallel circular beam is always assumed to be incident on the center of front of the first component module (i.e. at Z_min_CM(1)).

Based on the information in the literature [10-12], the parameters of the primary electron beam incident on the high Z target, including its energy and beam radius, were chosen to closely match the simulated beam profiles and percentage depth dose curves with the measured beam data.

Simulation parameters used for BEAMnrc and DOSXYZnrc were the Global cut off energy: for electrons ECUT= 0.70 MeV and for photons PCUT = 0.01 MeV. Electron range rejection and photon forcing was turned off for all simulations. Electron range rejection is used to save computing time during simulations where the range of charged particle is calculated and its history is terminated if it cannot leave the region it is in.

Photon forcing, where users force the photon to interact in a specific CM, improves statistics.

The cross section data for all material densities in the accelerator for particles with kinetic energy down to 10 KeV were from PEGS4 data file 700icru.pegs4dat.

Selective bremsstrahlung splitting was turned on to save simulation time. The minimum and maximum number of bremsstrahlung photons produced by each bremsstrahlung event was set to 20 and 200 brems photons. The effective field size in which selective bremsstrahlung splitting probabilities are calculated was set to 30 for the 10x10 cm^2 field and 50 for the 40x40 cm^2 field respectively. This technique improved the simulation time by a factor of 6 compared to no variance reduction.

Typically between 10^8-10^9 histories are needed depending on the pixel size in the X, Y and Z dimension in order to yield a statistically acceptable solution, as fewer numbers of particles interact in smaller volume.

2.3.7 Phase Space File

Phase space file is one of the most important outputs of BEAMnrc. Phase space file is a binary file and is usually tens of gigabytes of RAM in size. Information about each particle history including its charge, energy, position, direction of incidence and latch is stored in the phase space file. BEAMnrc outputs phase space file for planes that were

scored at the end of each component module, CM. The user specifies the desired plane for phase space file to be scored by making the selection in the BEAMnrc input file.

The phase space file can be used as a radiation source for further simulations in order to save time and hard disk space. For example, particles can be collected in the phase space file at the end of secondary jaws. The phase space file is then used as radiation source to simulate varying field sizes defined by MLC which is below the jaws (which is now the first CM as opposed to the target) or even downstream further away from the jaws where varying thickness compensators are simulated without having to resimulate the entire accelerator for each field size or compensator thickness, thus significantly speeding up the simulation.

The BEAM data processor BEAM-dp [14] was used to analyze the phase space files. The program was accessed using graphical user interface gui, beamdp_gui command in the accelerator directory. The program outputs the requested information such as fluence versus position, energy fluence versus position, energy fluence distribution, mean energy distribution, and angular distribution of the simulated electrons and photons in the phase space file which can be plotted for visual analysis.

The 6MV photon spectrum, the energy fluence distribution, mean energy distribution versus off axis distance for 10x10 and 40x40 cm^2 fields, fluence and energy fluence across the 10x10 cm^2 and 40x40 cm^2 fields, and the photon spectra were calculated.

2.3.8 Computer Cluster for MC Simulation

A Rocks 5.2 cluster of 22 computers has been used to accept independent batch jobs submitted by the MC code to the Q and distributed to local nodes by the master. The cluster runs Cent OS 5.3 distribution and is configured with 22 local nodes. One master server distributes the jobs to local nodes. Each compute node has two Xeon X5460 (3.2 GHz) Quad core processor with 32 GB memory. Compute nodes are interconnected by a private switch at 1 Gbps. Each compute node can handle simulation calculations independently of other nodes, therefore as many as 176 independent simulation jobs can be run simultaneously.

2.4 Results

2.4.1 Comparison Between Measured and Calculated Percent-Depth-Dose (PDD) Curves

Good agreement (± 1% or ±1 mm) is seen between calculated PDD curves (circle) for all beam energies (5.7, 6, 6.3MeV) and measured 6MV PDD curves (solid line) for (a) 10x10 cm^2 and (b) 40x40 cm^2 fields in the buildup to 5 cm depth range as in Figures 3 (a,b), 4 (a,b) and 5(a,b). The calculated PDD curves for 5.7 MeV beam were 1-2% lower than measured 6MV PDD curve beyond 5 cm depth for 10x10 and 40x40 cm^2 fields as in Figure 3 (a,b).
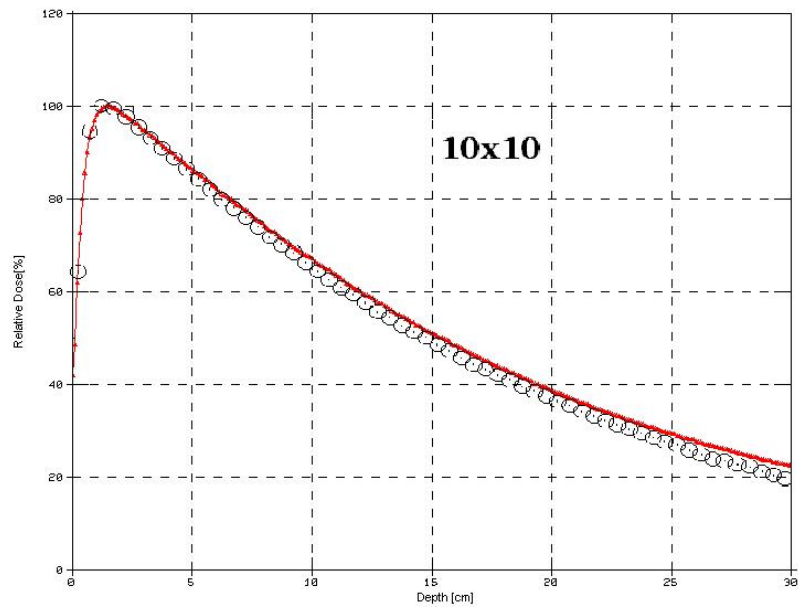
(a)
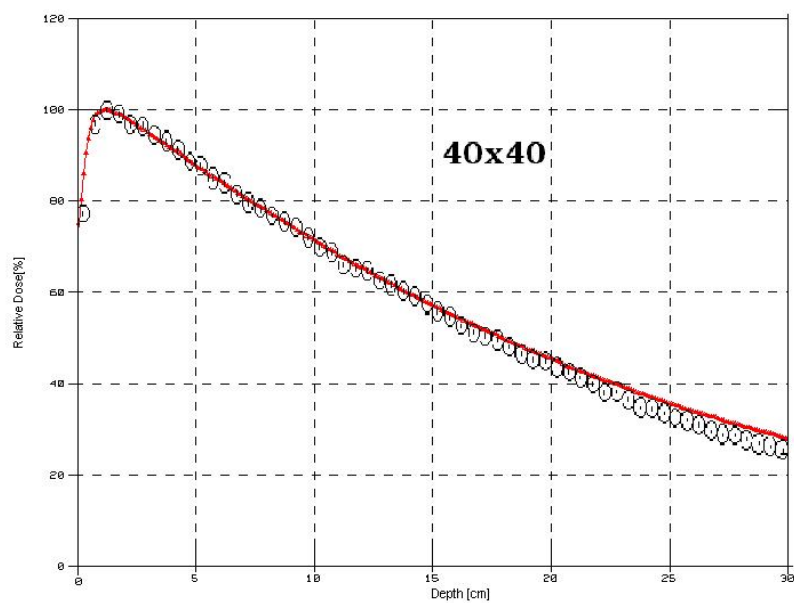
(b)

Figure 3. Overlay of measured 6MV photon depth dose curves (solid line) and Monte Carlo (circle) for 100 cm SSD and field size (a) 10x10 cm^2, and (b) 40x40 cm^2 calculated with 5.70 MeV electron beam incident on the target.

16
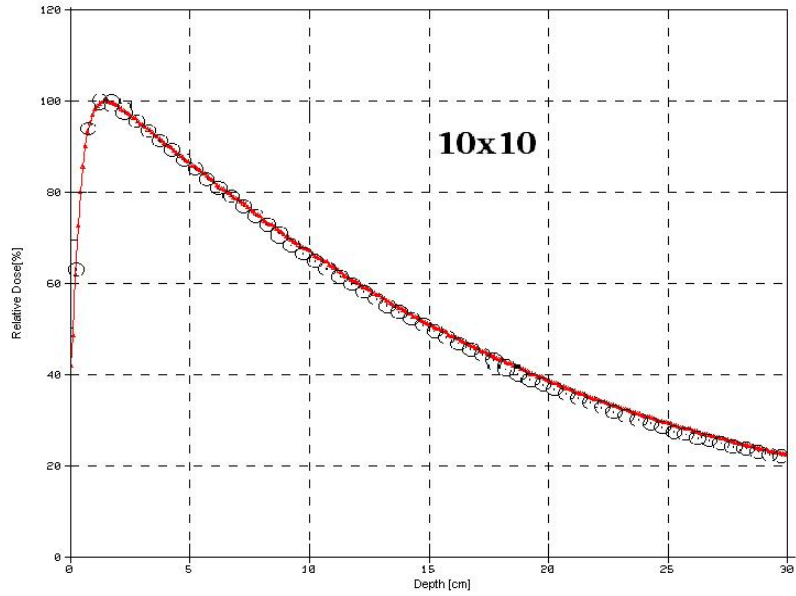
(a)
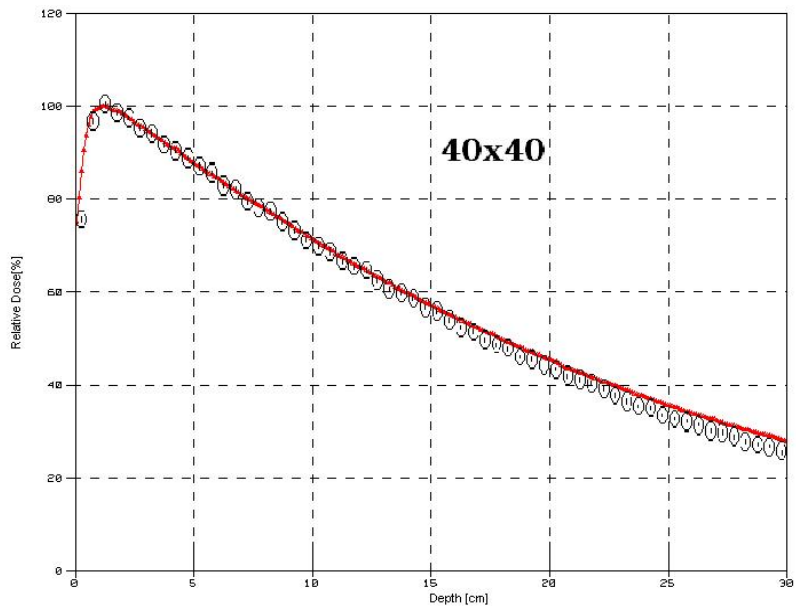
(b)

Figure 4. Overlay of measured 6MV photon depth dose curves (solid line) and Monte Carlo (circle) for 100 cm SSD and field size (a) 10x10 cm^2, and (b) 40x40 cm^2 calculated with 6.0 MeV electron beam incident on the target.
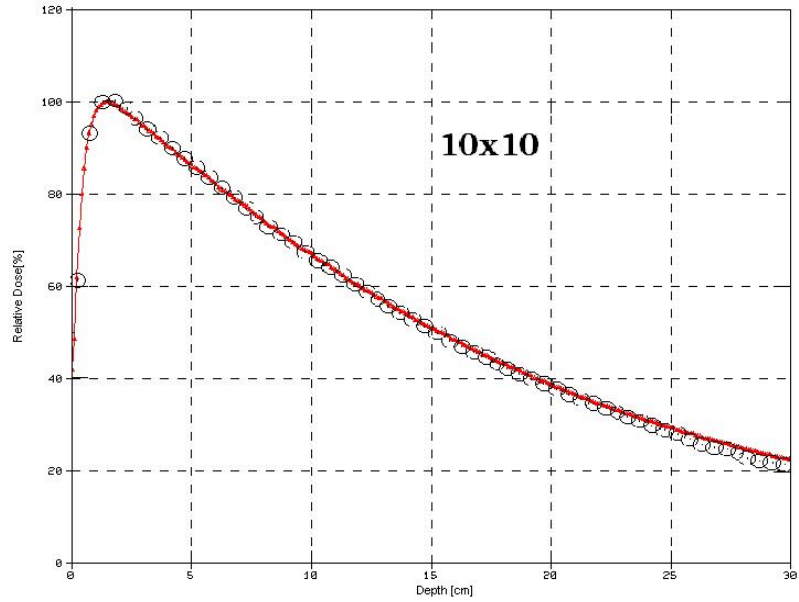
(a)
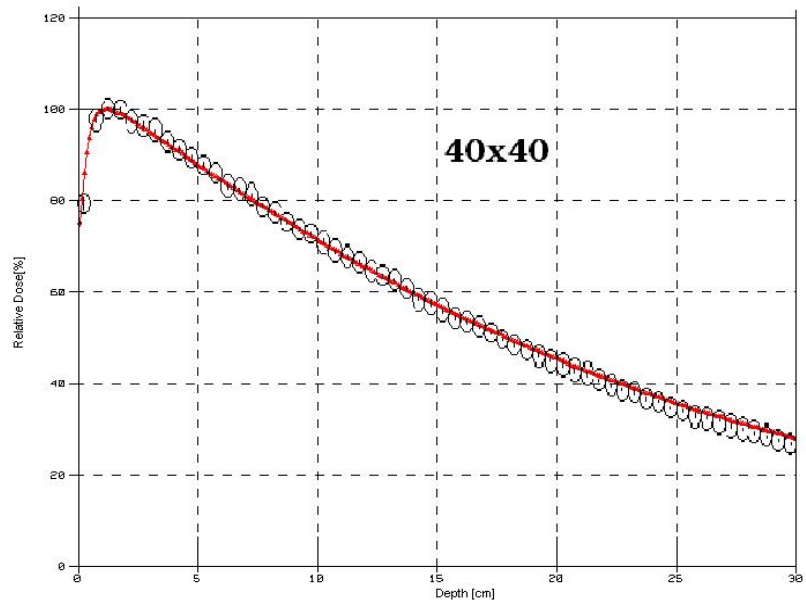
(b)

Figure 5. Overlay of measured 6MV photon depth dose curves (solid line) and Monte Carlo (circle) for 100 cm SSD and field size (a) 10x10 cm^2, and (b) 40x40 cm^2 calculated with 6.30 MeV electron beam incident on the target.

2.4.2 Comparison Between Measured and Calculated Beam Profiles

2.4.2.1 10x10 cm^2 Beam Profile

For 10x10 cm^2 fields, good agreement is seen between the measured 6MV beam profiles (solid line) and calculated (circle) beam profiles of the same fields at dmax, 5 cm and 10 cm depth for beam energies of 5.7 MeV as in Figure 6 (a-f), 6.0 MeV in Figure 7 (a-f), and 6.3 MeV in Figure 8 (a-f) respectively.

The agreement between measured and calculated beam profiles for 10x10 cm^2 beam at dmax, 5 and 10 cm depth was (± 1% or ±1 mm) as in Figures 6 (a,c), 7 (a,c,e) and 8 (a,c, e).for all beam energies and depths except 5.7 MeV beam profile at 10 cm depth was 1-2% lower than that measured as in Figure 6(e). There was also a small increase in the size of the horn at dmax for the 5.7 MeV beam, as in Figure 6(a).

2.4.2.2 40x40 cm^2 Beam Profile

For the 40x40 cm^2 fields, there was good agreement (± 1% or ±1 mm) between measured 6MV beam profiles and calculated beam profiles of 6.0 MeV and 6.3MeV beams for most depths, as in Figures 7 (b,d,f) and 8 (d,f), except 6.3 MeV beam profile at dmax was 1-2% lower than measured as in Figure 8 (b). The calculated 5.7 MeV beam profile, however, exhibited +6% increase in the size of the horn at all depths compared with the 6MV measured beam profile for 40x40 cm^2 field, as in Figure 6 (b,d,f).
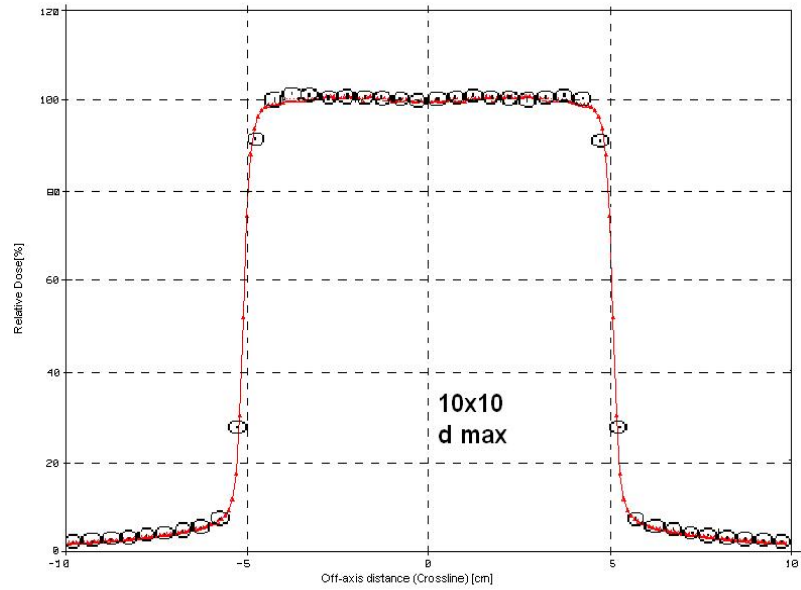
(a)
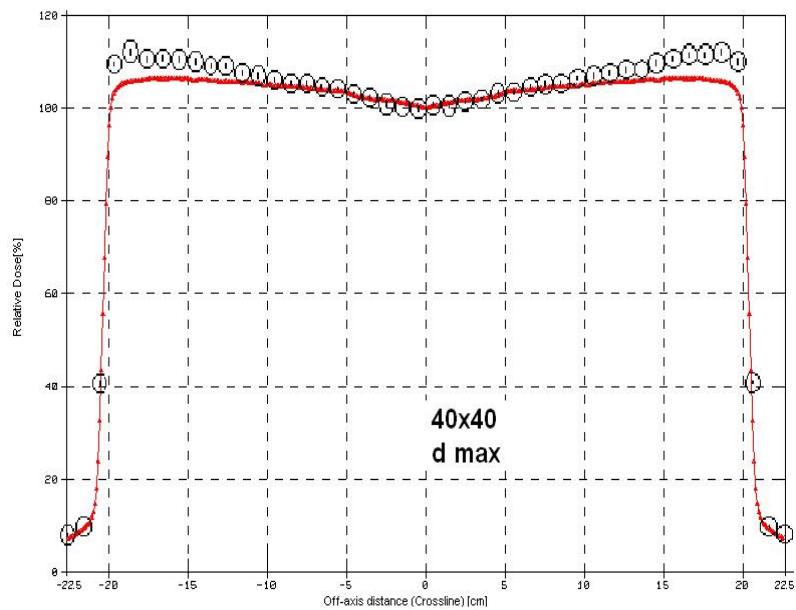
(b)

Figure 6. Overlay of measured 6MV photon beam profile (solid line) and Monte Carlo (circle) for 10x10 and 40x40 cm^2 fields at 100 cm SSD and at depths dmax (a, b), 5 cm (c, d) and 10 cm (e, f) in water, with simulated electron beam energy incident on the target was 5.70 MeV.
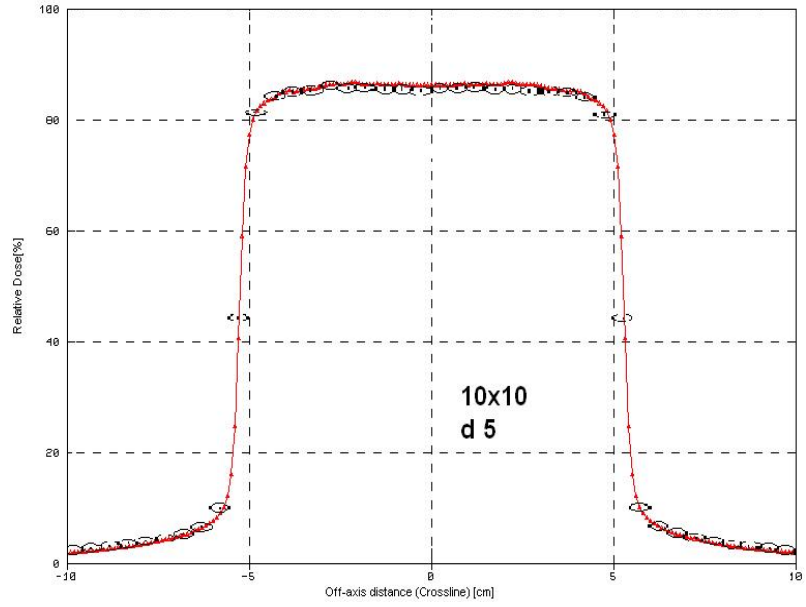
(c)
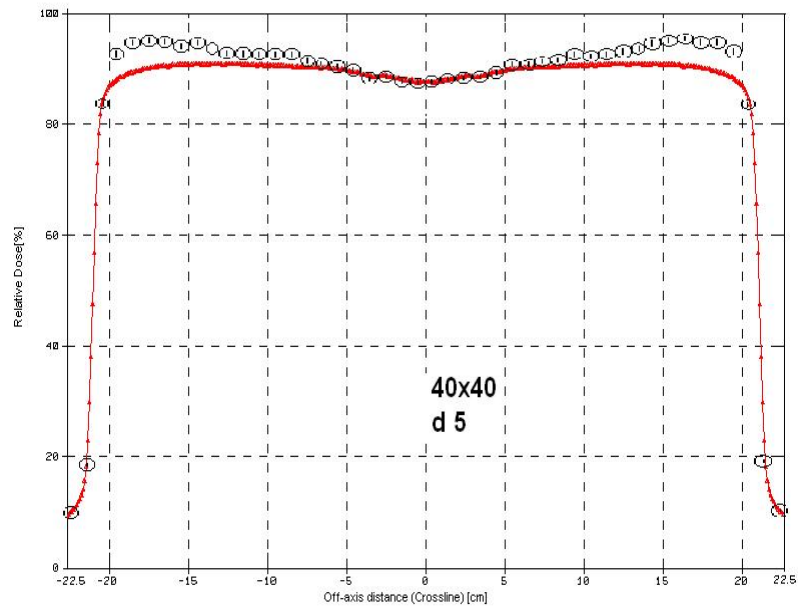
(d)

Figure 6. (Continued)

21
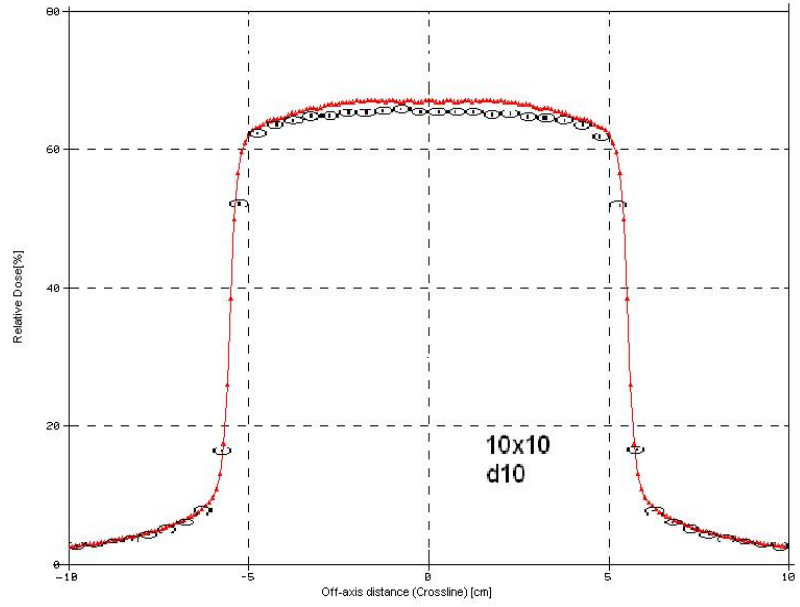
(e)
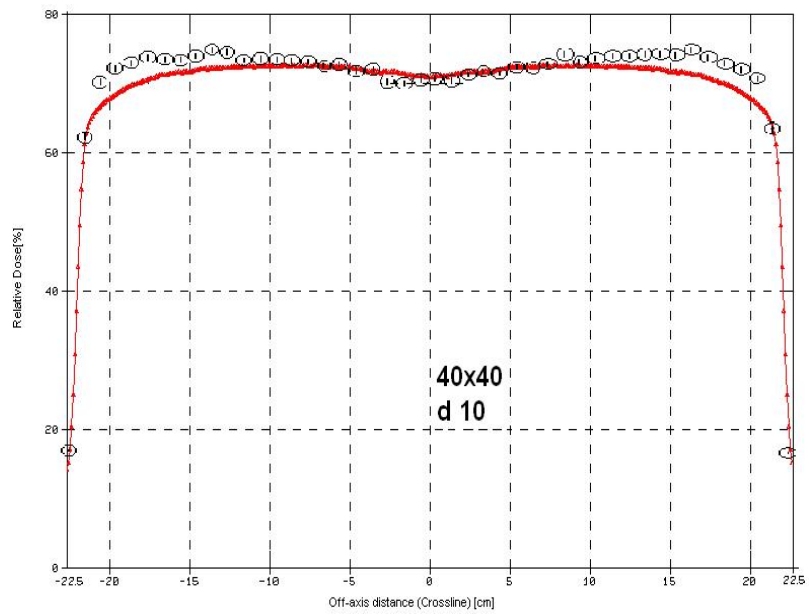
(f)

Figure 6. (Continued)
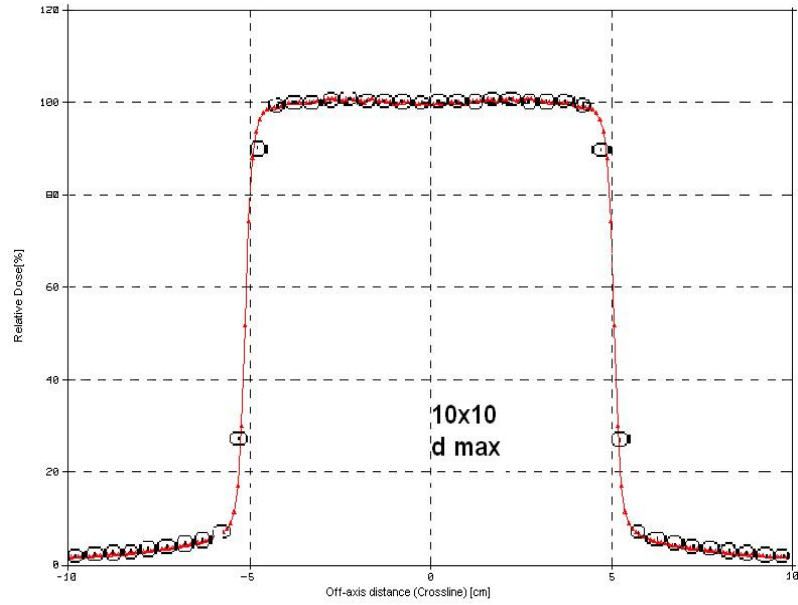
(a)
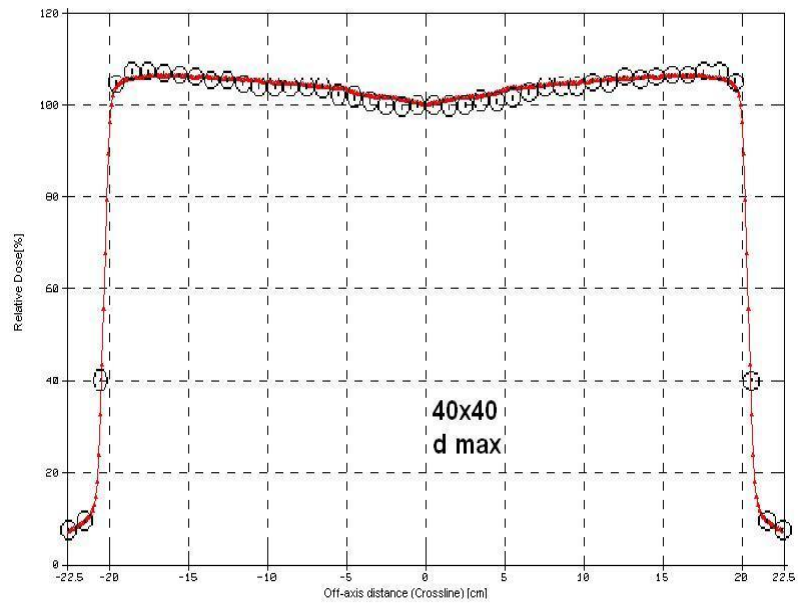
(b)

Figure 7. Overlay of measured 6MV photon beam profile (solid line) and Monte Carlo (circle) for 10x10 and 40x40 cm^2 fields at 100 cm SSD and at depths dmax (a, b), 5 cm (c, d) and 10 cm (e, f) in water, with simulated electron beam energy incident on the target was 6.0 MeV.

23
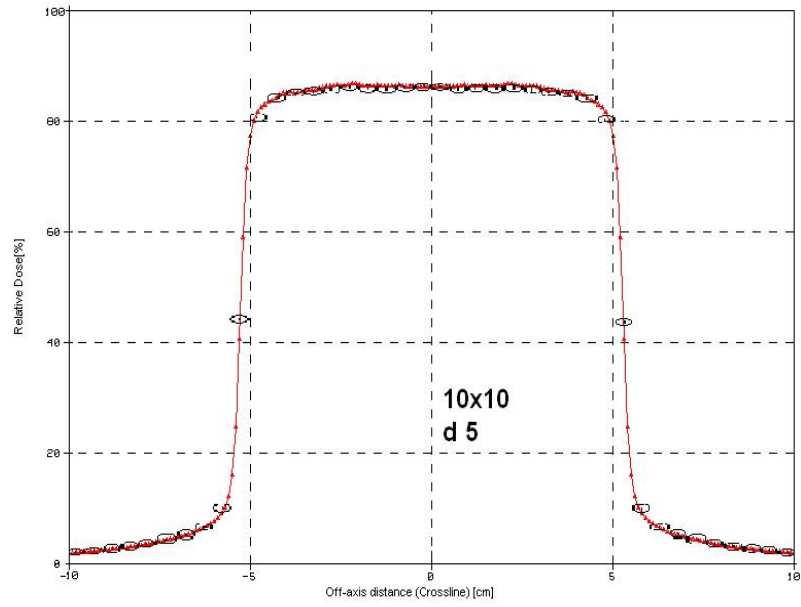
(c)
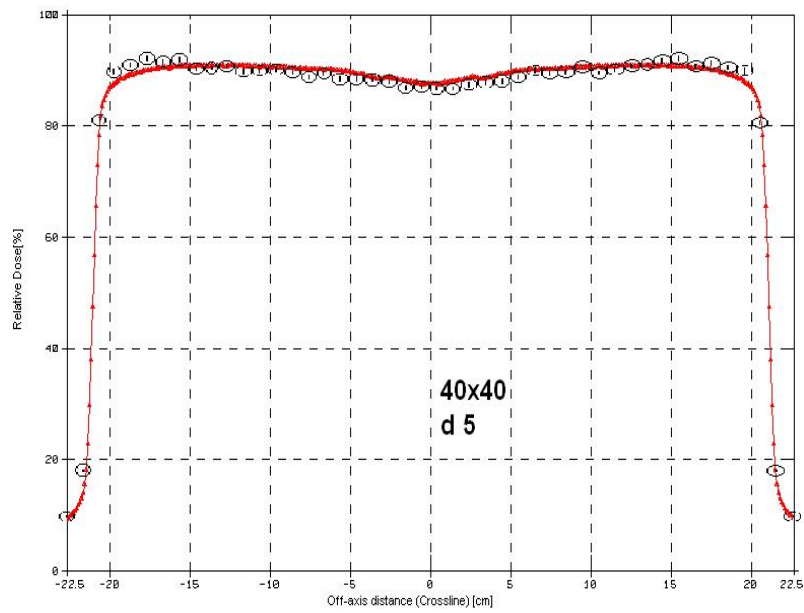
(d)

Figure 7. (Continued)
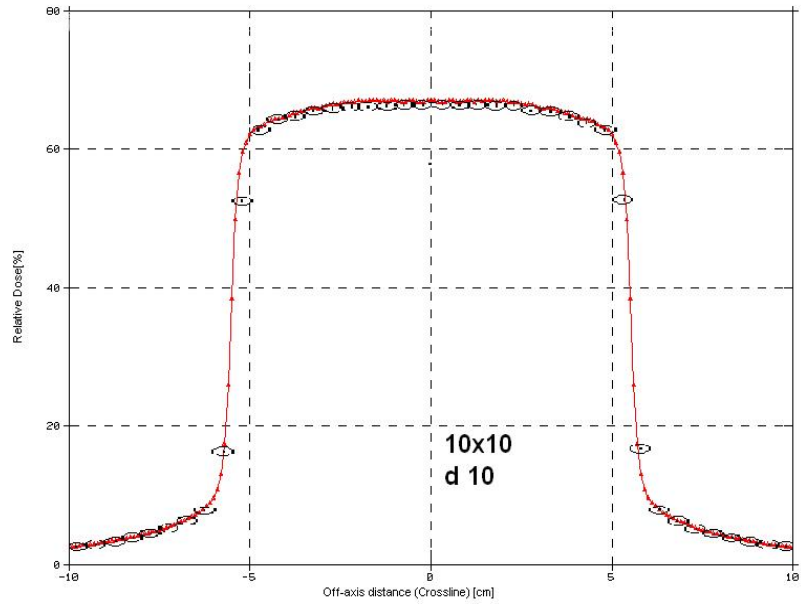
(e)
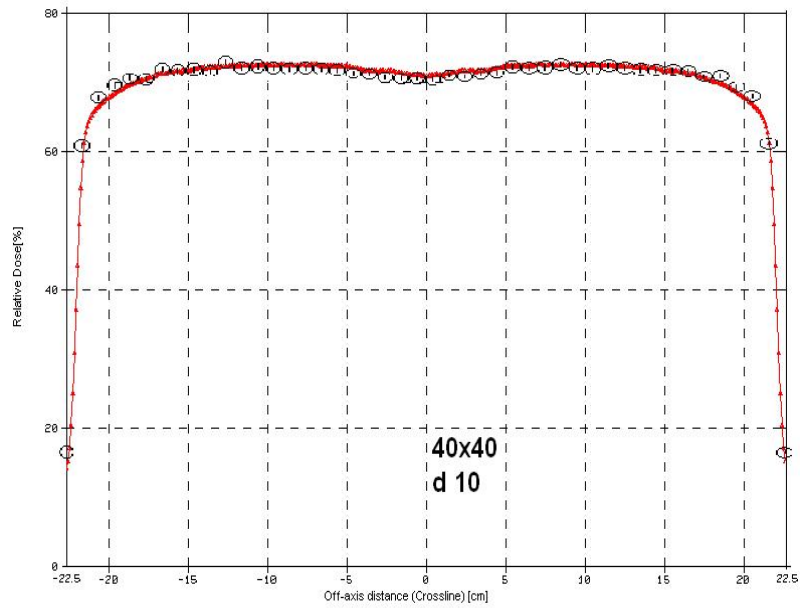
(f)

Figure 7. (Continued)

25
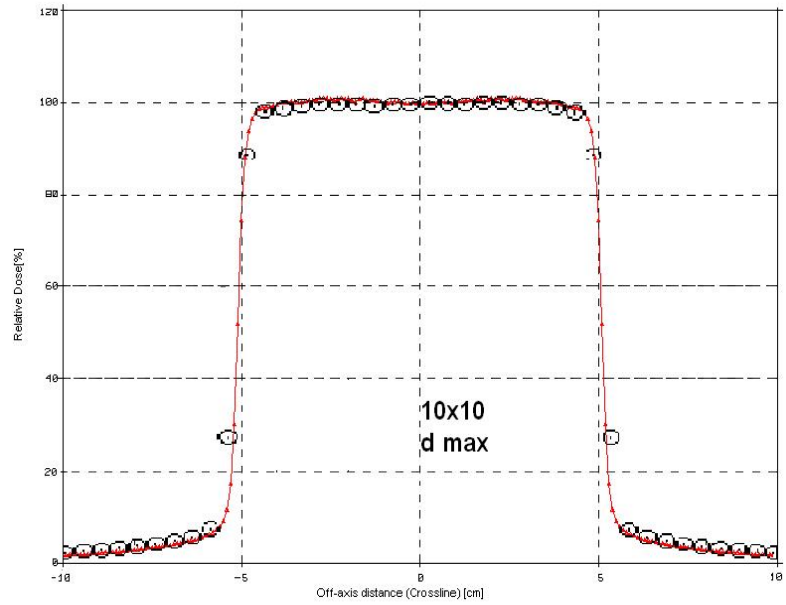
(a)
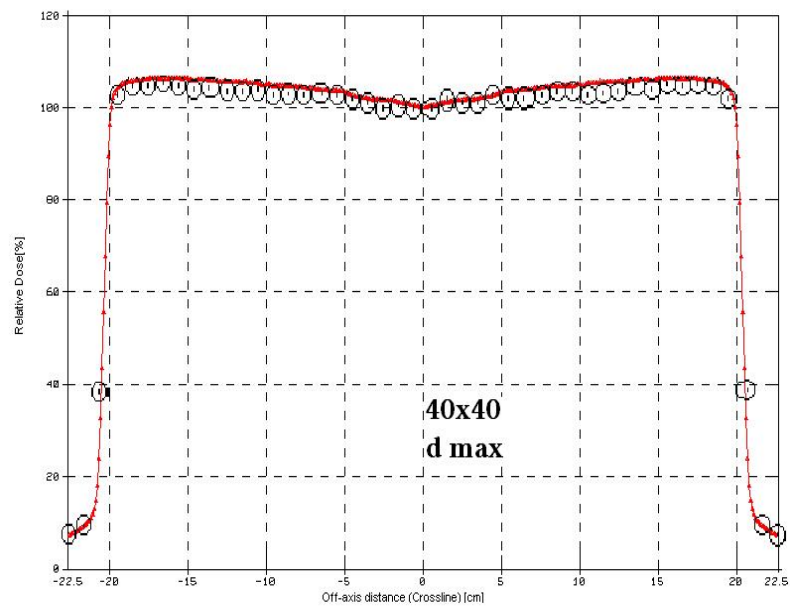
(b)

Figure 8. Overlay of measured 6MV photon beam profile (solid line) and Monte Carlo (circle) for 10x10 and 40x40 cm^2 fields at 100 cm SSD and at depths dmax (a, b), 5 cm (c, d) and 10 cm (e, f) in water, with simulated electron beam energy incident on the target was 6.30 MeV.
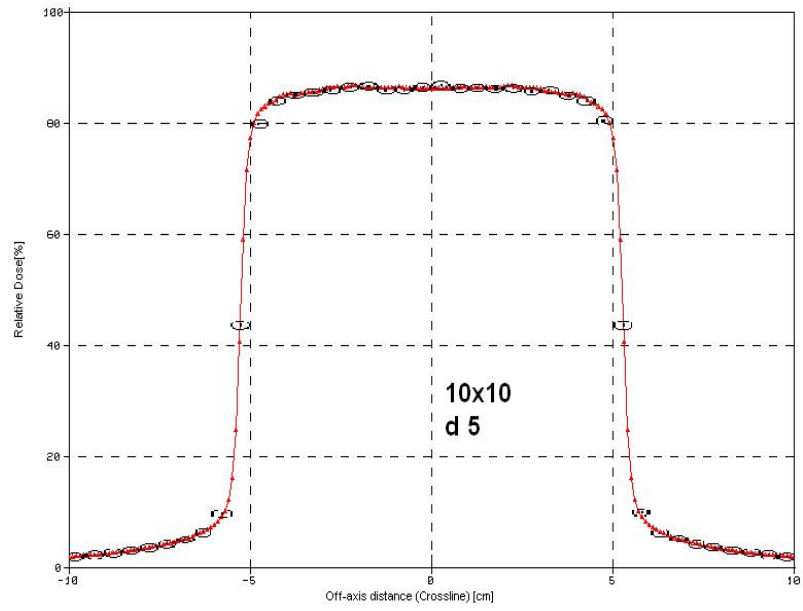
(c)
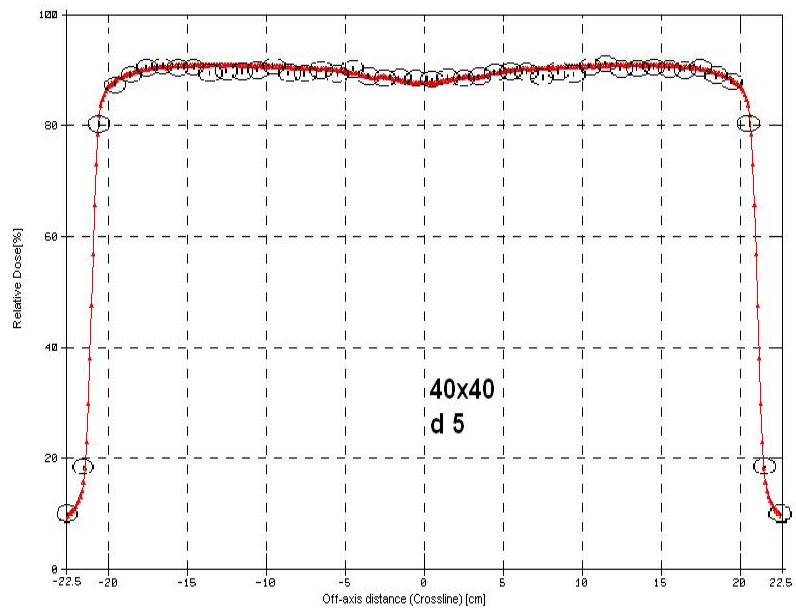
(d)

Figure 8. (Continued)
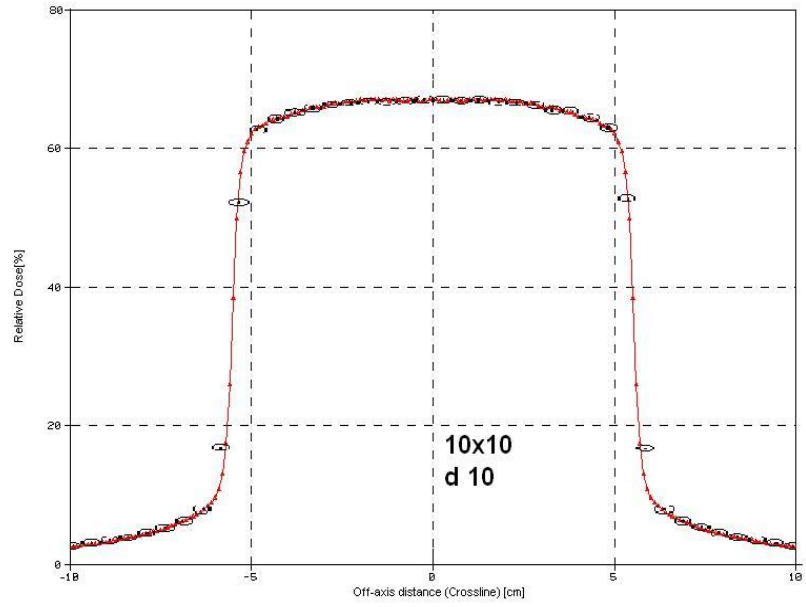
(e)
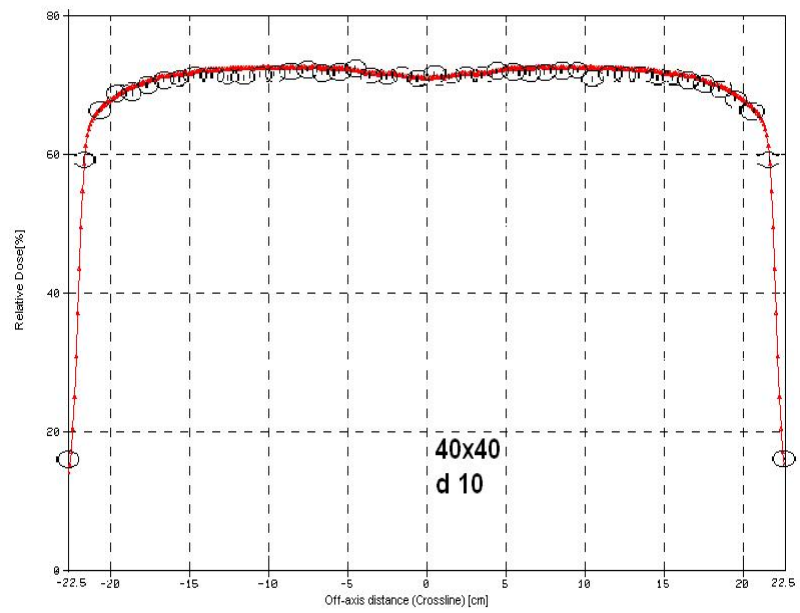
(f)

Figure 8. (Continued)

2.4.3 6MV Spectrum and Fluence

The photon spectrum calculated here for the region $0 \leq r \leq 3$ cm inside a 10x10 cm^2 field at 100 cm SSD is shown in Figure 9.

Figure 10 shows the energy fluence distribution for the 5.7, 6.0 and 6.3 MeV beam calculated at the surface of the phantom at 100 cm SSD, 10x10 cm^2 field of mixed photons and charged particles. The 5.7 MeV, 6.0 MeV and 6.3 MeV electron beam striking the bremsstrahlung target resulted in mean energy of 1.45 MeV, 1.55 MeV and 1.58 MeV beam at the phantom surface respectively.

Figure 11 (a) shows that the mean energy distribution at the phantom surface for 10x10 cm^2 field is relatively flat compared to that for 40x40 cm^2 field. Figure 11 (b) shows the mean energy distribution across 40x40 cm^2 field decreased with off axis distance toward the field edge. The mean energy at the field edge was 0.25 MeV lower compared to that at central axis for all beams. There is more low energy scatter dose contribution near the field edge compared to central axis for large fields.

Figure 12 (b) shows the fluence increased with 20 cm off axis distance reaching 135 % of central axis, near the field edge. These are mostly lower energy particles that were attenuated by thinner part of the flattening filter toward the field edge resulting in relatively flat energy fluence profile across the 40x40 cm^2 field, as in Figure 13.

Figure 13 shows the size of the horn of energy fluence profile across 40x40 cm^2 field decreased with increasing energy of primary electron beam incident on the target. This is because the relative intensity of photons increases with energy. Fluence of forward directed photons down the axis at small angles increases with energy more than it does at larger angles and away from central axis toward the field edge. Therefore the size of the horn decreases with increasing energy, as seen in Figure 13.
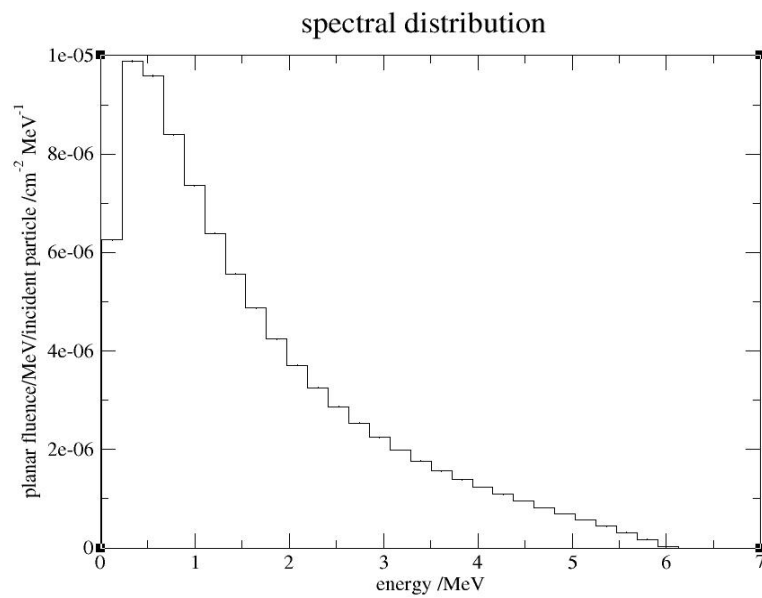
Figure 9. Calculated photon spectrum in the form of planar fluence histogram for the region $0 \leq r \leq 3$ cm inside a 10x10 cm^2 field at 100 cm SSD.
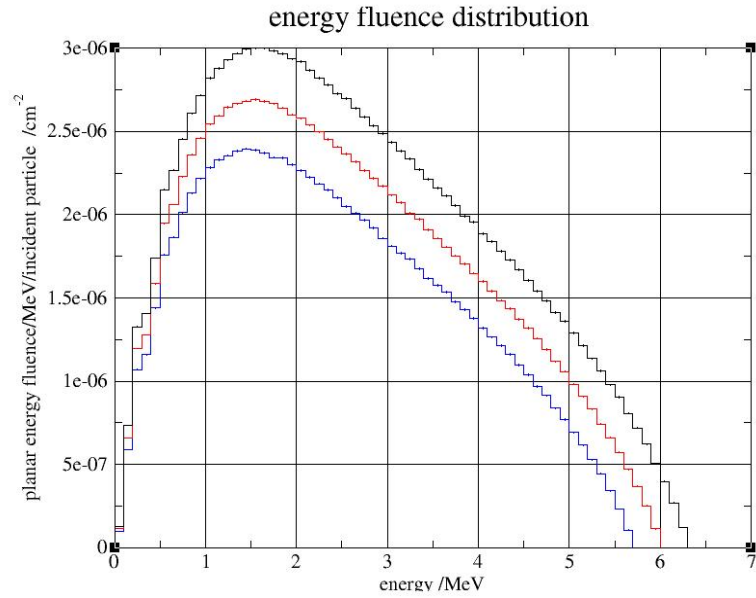
Figure 10. Calculated energy fluence distribution for 10x10 cm^2 field. The simulated electron beam energy incident on the target was 6.30 MeV top curve, 6.0 MeV middle curve and 5.7 MeV the bottom curve.

mean energy distribution

(a)

mean energy distribution
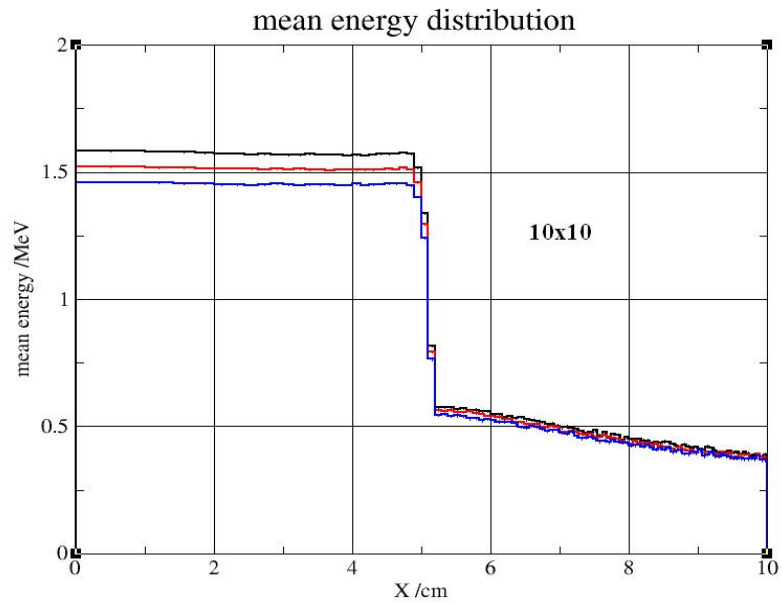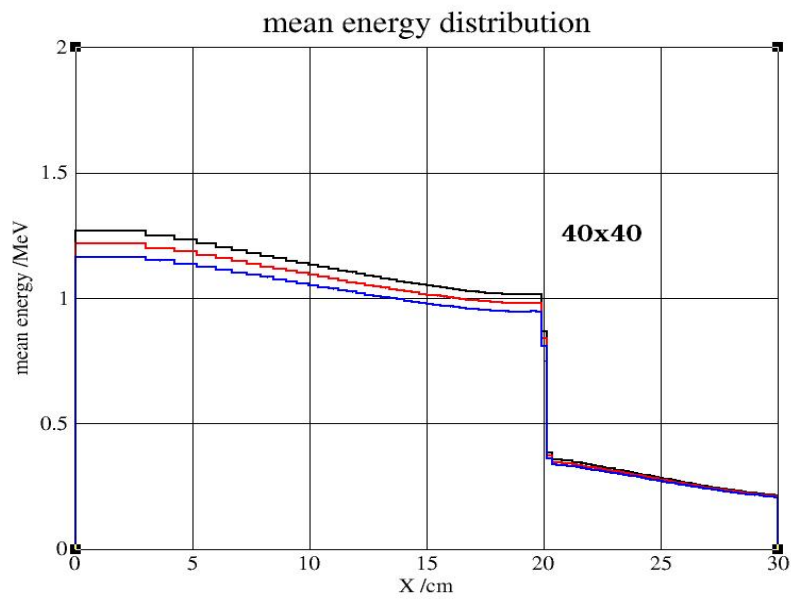
(b)

Figure 11. Calculated mean energy distribution across (a) 10x10 cm^2 field and (b) 40x40 cm^2 field. The simulated electron beam energy incident on the target was 6.30 MeV top curve, 6.0 MeV middle curve and 5.7 MeV the bottom curve.
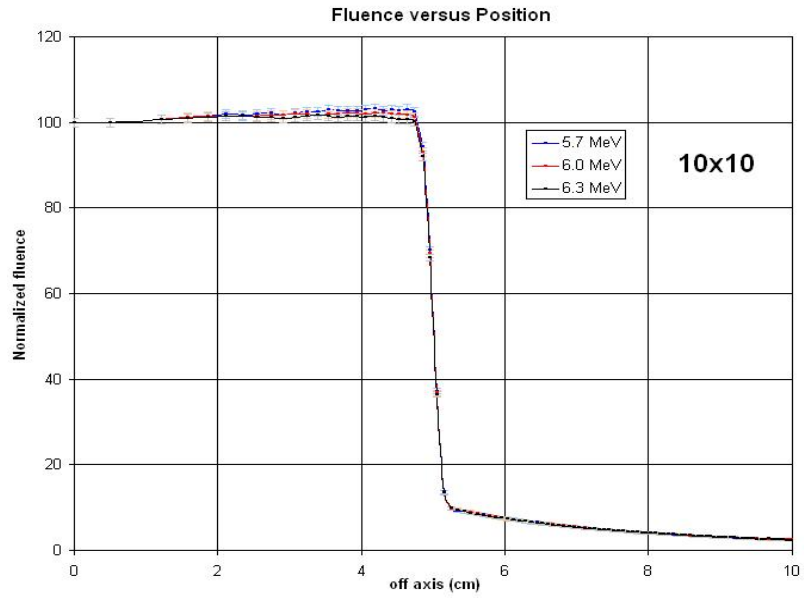
(a)
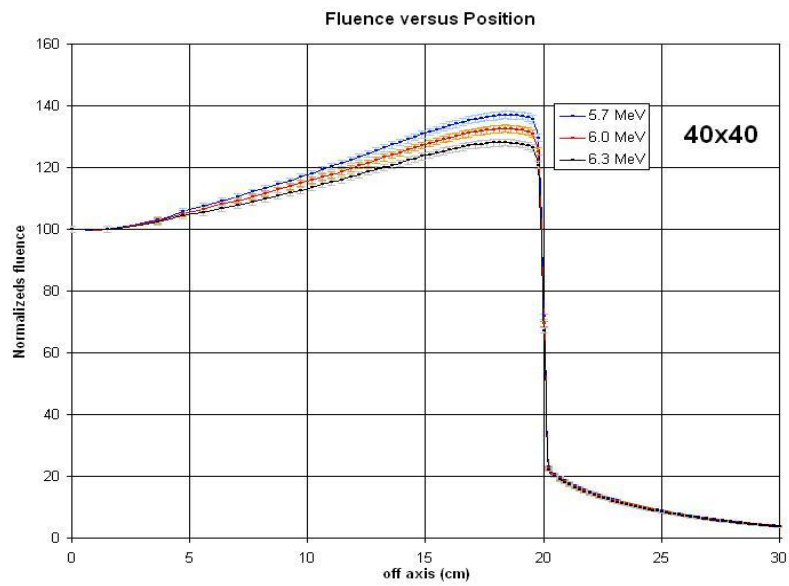
(b)

Figure 12. Calculated fluence versus position for (a) 10x10 cm^2 and (b) 40x40 cm^2 field. The simulated electron beam energy incident on the target was 5.7 MeV top curve, 6.0 MeV middle curve and 6.3 MeV the bottom curve.
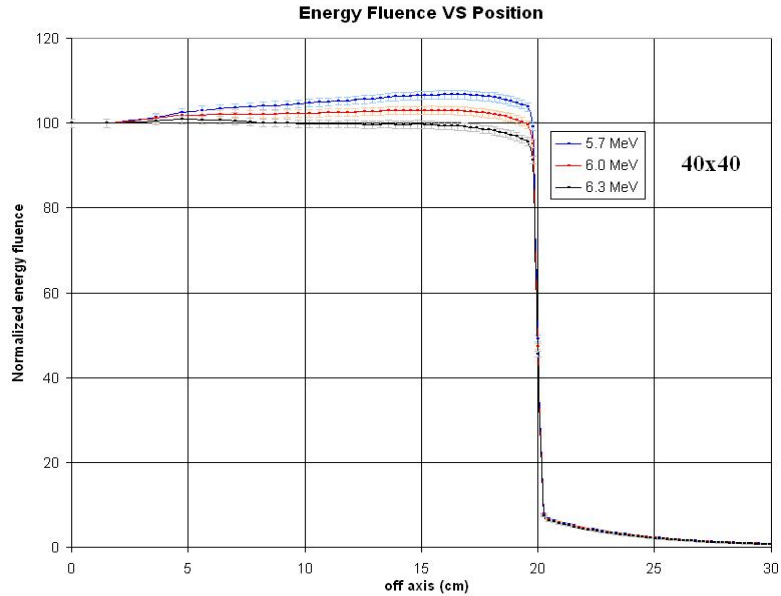
Figure 13. Calculated energy fluence versus position for 40x40 cm^2 field. The simulated electron beam energy incident on the target was 5.7 MeV top curve, 6.0 MeV middle curve and 6.3 MeV the bottom curve.

2.5 Conclusions

Since the calculated percentage depth dose and 10x10 cm^2 beam profiles were not as sensitive to changes in primary electron beam energy as were the large beam profiles, the match between measured and calculated 40x40 cm^2 beam profiles were used to find the optimum electron beam parameters in commissioning of the BEAM.

The optimum electron beam incident on the target had a radius of 1 mm with energy of 6.0 MeV respectively.

CHAPTER 3 PAPER I: SKIN DOSE STUDY OF CHEST WALL TREATMENT WITH TOMOTHERAPY

This study compares the dosimetric differences between TomoTherapy chest wall irradiation and traditional linear-accelerator-based tangential-beam technique. TomoTherapy treatment plans with and without bolus were compared with tangential-beam plans. Plans were also generated for phantom studies and point doses were measured using MOSFET dosimetry to verify the adequate skin dose. Monte Carlo simulations of static beams of both techniques were performed and dosimetry was compared.

(Jpn J Radiol. 2009; 27:355-362)

3.1 Synopsis

The tangential-beam technique frequently presents challenges in radiation dose homogeneity to the target. To ensure adequate dose to the skin, bolus is often used. TomoTherapy has already been shown to improve target conformity and homogeneity in other disease sites[16, 17]. Because of the tangential delivery technique and lack of flattening filter in TomoTherapy accelerators, we hypothesize that during chest wall irradiation using TomoTherapy, the skin dose will be adequate without bolus. Monte

Carlo simulations and measurements confirmed that beams from TomoTherapy deliver higher skin dose than a standard linear accelerator. Skin dose also increases with the incident angle of the beams. Due to the characteristics of the TomoTherapy beam and delivery technique, chest wall treatment plans from TomoTherapy showed adequate skin dose (over 75% of prescribed PTV dose) even without bolus.

3.2 Introduction

Many treatment modalities and techniques are available for the post-mastectomy radiotherapy to treat the chest wall[18-20]. The most commonly used technique is opposed tangential external beams to cover all the potential tumor-bearing chest wall tissues[21]. A supraclavicular field may be needed to adequately cover the regional nodes, if they are at risk[22]. Adequate treatment of the chest wall using the tangential-beam technique requires:

1. Homogeneous dose distribution over the chest wall;

2. Minimal dose to lungs, the opposite breast, and the heart;

3. Precise matching between the inferior border of the supraclavicular field and the superior border of the tangential fields;

4. Adequate dose to skin and the mastectomy scar (about 75%~90% of the prescribed dose);

5. Adequate dose to the axillary and internal mammary nodes (45~50Gy), when they are at risk[21, 23]..

These requirements often present challenges for the treatment planning. For example, although photon beams of 6MV and lower provide adequate skin dose without using bolus every day, there can be poor dose homogeneity, especially if the chest wall separation is large[21]. Higher energy photon beams improve dose homogeneity for large patients, but then bolus must be added to raise the skin dose. Use of bolus has also been associated with increased acute skin toxicity[24]. Common practice for chest wall treatments is to use bolus every other day, even with 6MV photon beams. It is important to note that if the bolus and non-bolus plans are rotated, then the goal is not to have 100% prescribed dose at the surface, but something closer to 80% of the prescribed dose. Superficial dose ranged from 74% to 93% by phantom measurement when incident beam angle varied from 0 to 90 degrees with bolus on/off alternatively[25].

Previous investigators have shown that TomoTherapy Hi-Art (TomoTherapy Inc., Madison, WI) provides an advantage in a higher skin dose by using skin flash beams. Other clinical researchers have demonstrated that TomoTherapy planning usually overestimates superficial dose by up to 10% for shallow planning target volumes (PTV)[26, 27] which needs to be accounted for while evaluating the skin dose in TomoTherapy plans. However, good agreement (<2.5%) between calculated and measured skin dose has also been reported[28].

The area at risk represents some combination of the basal layer of the skin and the dermal layer which contain the dermal lymphatics[29], and potential cancer cells within the lymphatics. Thus, the area at risk which is targeted is not on the surface, but 1 to 5 mm

below the surface. Besides the superficial dose as studied by other groups[30], the focus of this study extends to dose gradient at shallow depths in the chest wall.

In this study, clinical cases of chest wall treatment plans are compared. Phantom studies were also performed to compare the skin dose differences between the treatment techniques. Measurements of skin dose were compared with treatment plans. Monte Carlo simulations were also used to confirm the skin dose differences.

3.3 Material and Methods

3.3.1 Patient Cases

A total of 5 previously treated chest wall patients were selected for treatment plan comparison. Treatment plans were generated for TomoTherapy and conventional tangential-beam technique. Besides PTV radiation dose coverage, dose distributions for lungs and heart were also evaluated. However, the skin dose is the primary planning parameter in this comparison.

3.3.2 TomoTherapy Planning

Clinical cases of chest wall treatment plans and phantom plans to simulate chest wall treatment were generated and studied. A collapsed cone convolution/superposition algorithm[31] was used for all the plans. Heterogeneity corrections were applied.

The pitch value in all the plans was set at 0.287. The modulation factor was 2.7. The plan objective was at least 95% of the PTV volume to receive the prescription dose of 50 Gy. Heart dose was limited such that less than 5% of heart volume received less than 20 Gy. Lung dose constraints were: less than 25% of the ipsilateral lung volume received 15 Gy and less than 15% of the contralateral lung received 2.5 Gy. Directional blocks were used in the TomoTherapy plans to reduce the dose to the lungs and heart. TomoTherapy plans without directional blocks were also generated for comparison.

Treatment plans for a Rando Man phantom (The Phantom Laboratory, Salem, NY) were also generated for skin dose measurements. A Rando phantom is constructed with materials equivalent to soft tissues and skeleton. It simulates realistic human anatomical structures. Figure 14 shows examples of the plans.
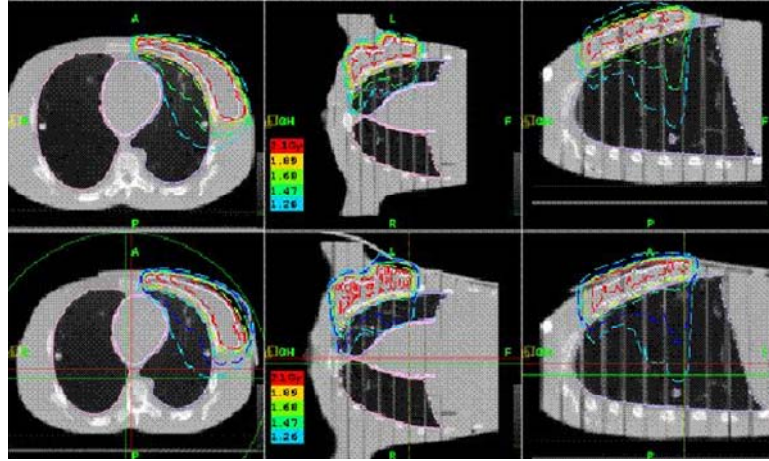
Figure 14. The TomoTherapy chest wall treatment plans on a male Rando phantom. The upper row shows the transverse, coronal and sagittal views of the plan without a bolus, and the lower row shows the plan with a bolus. These plans were generated for the skin dose measurement using MOSFET dosimeters. Air gaps under the bolus are noticeable on the images of the plan with a bolus.

3.3.3 Tangential-Beam Planning

Tangential-beam plans of clinical cases were generated using the XiO planning system (Version 4.34.02.1, CMS, Inc, St. Louis, MO) for an Oncor linear accelerator (Siemens Medical Solutions USA, Inc. Malvern, PA). Two tangential beams were used in the plans. Field-in-field technique[32] was used in some of the tangential-beam plans to improve PTV dose homogeneity. Electron beam was included in some of the cases to treat the internal mammary region. A superposition algorithm[33] was employed in the dose calculation. Heterogeneity correction was turned on to account for lung and bone densities. The same contour set of target volumes and critical structures used in each TomoTherapy plan was used in the corresponding tangential-beam plan. The photon beam energy used in the tangential-beam plans was 6MV, and the electron beam energy

was 9 or 12 MeV. Chest wall treatment plans were also generated on a Rando phantom for skin dose measurement.

3.3.4 Monte Carlo Simulation

An EGSnrc[7] based Monte Carlo simulation package for clinical radiation treatment units, BEAMnrc[34], was used to simulate linear accelerators with and without a photon beam flattening filter. The absence of a flattening filter in a TomoTherapy unit is one of the major differences compared to conventional linear accelerators. A total of 1×10^8 electrons with the incident energy of 6 MeV were simulated in each accelerator head. Phase space files, in which physical parameters of all the particles passing through the plane of interest is stored, were scored at the end of the secondary jaws. The phase space files were then used as radiation sources in phantom dose distribution calculations using DOSXYZnrc[13], another Monte Carlo simulation computer program for simple geometry media.

Another major difference between a conventional linear accelerator and Tomotherapy is that the source to axis distance (SAD), for a conventional linear accelerator is 100 cm while it is 85 cm for TomoTherapy. Therefore a difference of source to surface distance (SSD) of 15 cm was also compared in Monte Carlo simulations.

Dose in phantom versus radiation beam incident angle was studied to understand the dose effect at shallow depth of the helical delivery technique that TomoTherapy uses and

angled beams in tangential-beam technique. The beam size used in the simulation was 5×5 cm^2. The resolution of the dose grid along the central axis direction in the water phantom was $3\times3\times0.15$ cm^3, where 0.15 cm was along the direction perpendicular to the phantom surface. The rotation axis of the beams (isocenter) was at the phantom surface.

3.3.5 Dose Measurements

The mobileMOSFET TN-RD-16 wireless dose verification system (Thomson & Nielsen Electronics Ltd, now Best Medical Canada, Nepean, Ontario, Canada) was used for the dose measurements. According to the specifications, the system has an accuracy of 2% at 200 cGy dose level at standard bias.

The MOSFET readings were cross checked with ion-chamber measurements using the TomoTherapy monthly static output in reference geometry setup. With this setup[35], stationary dose delivery was used to deliver about 200 cGy to the depth of maximum dose, d_{max}, of a solid water phantom. Chamber reading and MOSFET reading were acquired simultaneously.

Point doses of the TomoTherapy plans were measured at the phantom surface and under 5 mm bolus. TomoTherapy and tangential-beam chest wall plans on the Rando phantom were delivered on a TomoTherapy unit and an Oncor linear accelerator respectively.

Treatment plans for a TomoTherapy® delivery quality assurance (DQA) phantom, known as cheese phantom, were also generated for this study. The cheese phantom was used because of the convenience of using a ready-pack film to measure the dose distribution including the "skin" dose. Kodak extended dose range (EDR) films were used to measure the skin dose gradient relatively. Figure 15 shows the measurement setup with film and MOSFET dosimeters. A Hurter and Driffield (H & D) curve was generated for this purpose. The exposed EDR film was scanned and the dose distribution image was analyzed on the TomoTherapy® planning system. The measured dose distribution was aligned with the planar dose distribution from the plan using the alignment tools in the planning system.
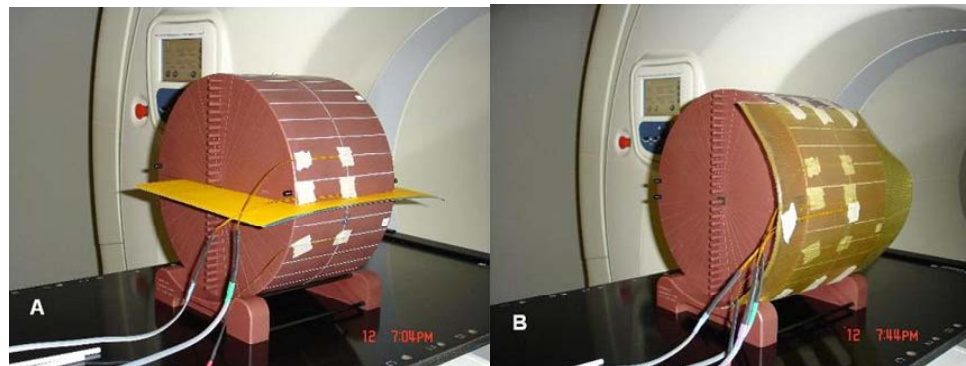
Figure 15.   Film and MOSFET dose measurement setup with TomoTherapy cheese phantom. Treatment plans were generated to simulate chest wall treatment. The treating region was along the edge of the phantom where MOSFET dosimeters were located.
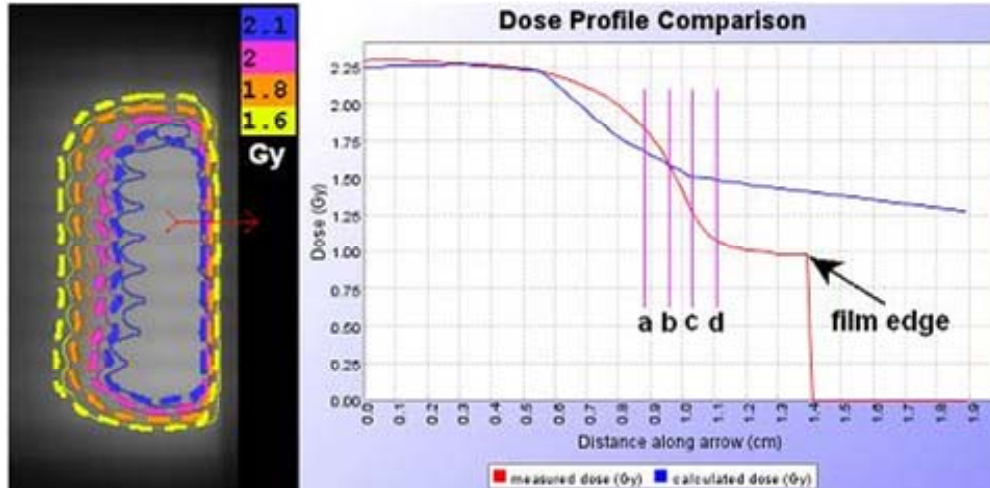
Figure 16. Dose gradient difference between the film measurement and the treatment plan. The real dose increases with depth much faster than that in the plan. Due to this difference and the coarse resolution in TomoTherapy treatment plans, a slight difference in phantom edge definition could cause a large range of dose variation between measurements and plans. In this figure, the difference between line a and d is about 2 mm, while the dose difference of the planned dose-measured dose ranges from -0.1 to +0.4 Gy.

3.4 Results

3.4.1 Film Dosimetry

The relative dose distributions measured using EDR film on the cheese phantom for chest wall treatment plans showed steeper dose gradient than that in TomoTherapy plans. Figure 16 is an example of the comparisons of the dose gradients between the planned and measured dose distributions. In this example, the shallow dose increased from 1.5 to 2.0 Gy in 2 mm depth. Due to the coarse spatial resolution in TomoTherapy planning system, one pixel misalignment between the film and the phantom image could introduce 2 mm spatial shift. If this spatial shift is along the high gradient direction, it corresponds

to a 0.5 Gy difference in superficial dose. The dose gradient difference between the film measurements and TomoTherapy plans could be the explanation to the wide variation of superficial dose differences reported by different groups[26-28] (see Figure 16). Also because of this difference, TomoTherapy planning is likely to overestimate the superficial dose. An important conclusion of the film dosimetry study is that the TomoTherapy planning may overestimate the superficial dose while it underestimates the dose gradient in shallow regions in chest wall treatment plans. In the example shown in Figure 16, the dose gradient of the measured dose is two times that of the planned dose in the high gradient region. The sharp dose gradient in chest wall treatment may cause higher skin dose (not superficial dose) than what the plan shows.
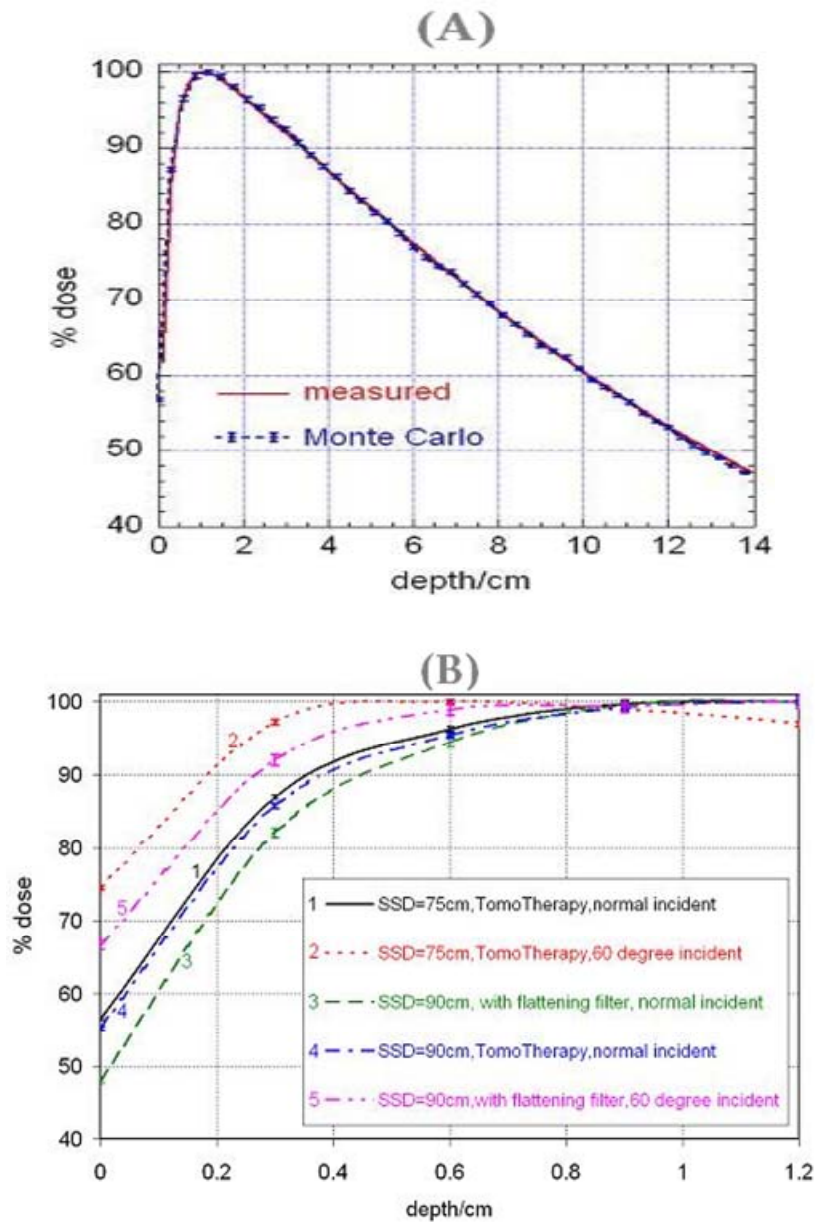
Figure 17. (A) Monte Carlo calculated TomoTherapy percentage depth dose (PDD) versus measured PDD. The SSD is 85 cm; (B) Monte Carlo calculated shallow depth dose distributions of a TomoTherapy machine and a conventional linear accelerator versus SSD and incident angle. The statistical uncertainty of the Monte Carlo calculated PDD is within 1% for all data points (see the error bars).

Table 1. Comparison of the measured superficial dose between TomoTherapy and tangential-beam techniques on a Rando phantom using MOSFET.

Technique	TomoTherapy			Tangential-beam		
Location	Surface	5mm bolus	Alternative	Surface	5mm bolus	Alternative
Dose (cGy)	152.4±6.1	205.6±9.7	179.0±5.7	134.0±8.0	188.5±5.5	161.3±4.9
% to 2 Gy	76.2±3.0	102.8±4.8	89.5±2.9	67.0±4.0	94.3±2.8	80.6±2.4

3.4.2 MOSFET Dose Measurement

The calibration of MOSFET against ion chamber was carried out using a TomoTherapy unit in stationary mode. The MOSFET readings differed with ion chamber readings by -1.51% ± 0.44%, within the manufacturer's specification.

Table 1 lists the measured point doses at phantom surface and under 5 mm bolus. The average dose of alternative bolus on/off was calculated using the measured doses. The measured superficial dose of the TomoTherapy plan (76.2% ± 3.0% of the prescribed PTV dose) is lower than the alternative bolus on/off dose of the tangential-beam technique (80.6% ± 2.4%) but comparable, while the alternative on/off dose from the TomoTherapy plan (89.5% ± 2.9%) is also within the adequate dose range. Considering the skin dose is actually not the superficial dose but at about 1 mm depth, and the sharp dose gradient in the shallow regions, this dose could be too high and likely to cause skin reactions.

3.4.3 Monte Carlo Study

Figure 17A shows the agreement of the measured and calculated PDD curves for the TomoTherapy machine. Figure 17B demonstrates the dose differences at shallow depth versus SSD and accelerator. The effect of the 15 cm difference in SAD between TomoTherapy and conventional accelerator can be seen in this figure. About 2% difference in dose is introduced by the SAD difference, with a higher superficial dose for a shorter SAD (the superficial dose difference between curves 1 and 4 in Figure 17B). The absence of the flattening filter increases the superficial dose by about 7% at the same SSD (Curves 3 and 4). The combination of the absence of a flattening filter and shorter SSD results in about an 8% higher superficial dose for TomoTherapy (Curves 1 and 3).

Tangential beams increase the superficial dose for both TomoTherapy beams and conventional accelerator beams. The Monte Carlo simulation shows that the magnitude of the increase is about the same for both TomoTherapy beams and conventional accelerator beams (Curve 2 versus Curve 1 for TomoTherapy beams and Curve 5 versus Curve 3 for conventional accelerator beams in Figure 17B). A 17% superficial dose increase can be observed in Figure 17B when the incident angle is changed from 0 to 60 degrees.

The shallower d_{max} in TomoTherapy beams with large incident angles is the major reason that the TomoTherapy chest wall treatment plans usually have higher skin dose than conventional tangential-beam plans.

3.4.4 Plan Analysis and Comparison

Figure 18 shows the skin dose comparison of a TomoTherapy plan without bolus to tangential-beam plans of with and without bolus. The same patient and same location was chosen for all the depth dose profiles of the TomoTherapy and tangential-beam plans. The superficial dose of the TomoTherapy plan was much higher than the average of the two tangential-beam plans. While Figure 17 shows the comparison for only one location, Table 2 lists more statistical data of the comparison, which shows even higher skin dose without bolus and less dose variation in the TomoTherapy plans compared to the conventional tangential-beam plans. Comparing the superficial doses listed in Table 2 with the ones in Table 1 which are the measurement data, an overestimation of superficial dose in TomoTherapy plans of about 12% can be concluded, while for the tangential plans, the overestimation is about 2%. Taking into account the overestimation of superficial dose by TomoTherapy, in the example shown in Figure 18, even without bolus, the corrected TomoTherapy plan (about 80% superficial dose) still provides adequate skin coverage, which agrees with the measurement data in Table 1 within 4%.
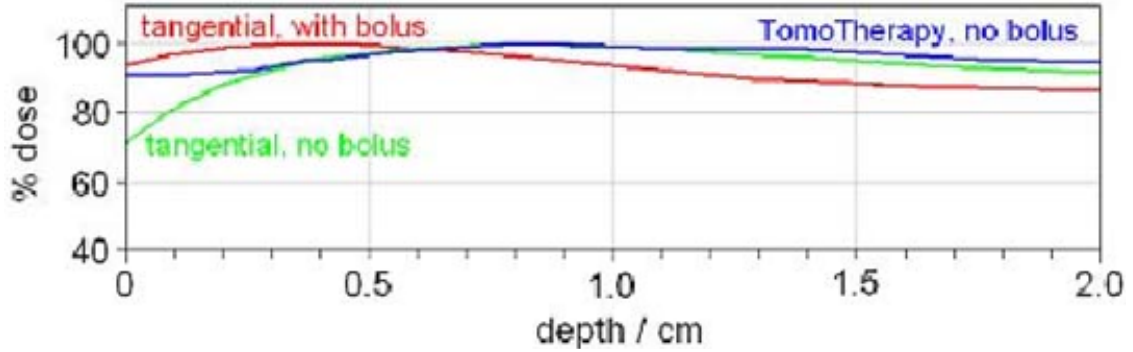
Figure 18. Skin dose comparison of TomoTherapy with tangential-beam technique. All dose profiles were obtained from treatment plans of the same left sided chest wall patient at the same location. The superficial dose of the TomoTherapy plan (without bolus) is between the ones of tangential plans with and without bolus.

Table 2. Normalized dose at the surface, 2 and 5 mm depth is compared for chest wall treatment plans using the tangential-beam technique and TomoTherapy. Dose at the surface and depth are normalized to the prescribed dose. A total of 20 points in treatment plans were chosen for each depth. The value shown in this table for each plan at each depth is the average and one standard deviation. Even without bolus, TomoTherapy plans usually have high superficial dose and dose at shallow depth (skin dose). The standard deviation in TomoTherapy plans is usually smaller than that in conventional tangential-beam plans, indicating more conformal dose distributions in TomoTherapy plans. The overestimation of superficial dose in the plans is not corrected in this table.

Plan	% superficial dose	% dose @2mm	% dose @5mm
Tangential, no bolus	69 ± 6	85 ± 5	97 ± 3
Tangential, bolus	83 ± 7	87 ± 4	95 ± 2
TomoTherapy , no bolus	88 ± 3	92 ± 4	94 ± 4
TomoTherapy , bolus	102 ± 3	104 ± 2	101 ± 2

3.4.4.1 Discussion

A possible problem associated with bolus is that there may exist air gaps between the bolus and chest wall (Figure 14) which could further vary in daily treatments. This variation would introduce uncertainty in delivered dose. Especially for TomoTherapy, the variation of daily bolus location could introduce dose uncertainty due to its helical delivery technique. However, bolus has been suggested as desirable for TomoTherapy to reduce the effect of daily setup error and potential underdosing of the surface[36], and to correct for shallow depth dose overestimation in TomoTherapy treatment planning algorithm[26].

Due to the angular dependence of MOSFET dosimeters (3.0-3.5%), their measurement uncertainties (2-3%) and other possible setup errors, the estimated accuracy of MOSFET dosimetry is about ± 6%[37]. The estimated 12% overestimation of TomoTherapy treatment planning system may include the MOSFET measurement uncertainty.

Based on the measurement data, TomoTherapy without bolus delivers adequate skin dose but it is lower than what the alternative bolus on/off plan of tangential-beam technique delivers (76.2% ± 3.0% of prescribed PTV dose versus 80.6% ± 2.4% to skin surface). TomoTherapy alternative plan also delivers adequate skin dose (89.5% ± 2.9% to skin surface) but at the high limit. A scheme of two days without bolus and one day with bolus in TomoTherapy gives a moderate superficial dose (85.1% ± 2.6%).

3.5 Conclusion

Compared to a tangential-field technique, TomoTherapy shows a higher superficial dose in chest wall treatment without using bolus in both treatment plans and measurements. The reasons of the higher superficial dose are 1) slightly lower mean energy than a conventional linear accelerator and therefore a shallower d_{max}, 2) shallow delivery angles used in the treatment delivery, and 3), the smaller SAD of the TomoTherapy unit. Therefore it is a reasonable clinical practice to treat chest wall on TomoTherapy without using bolus, or using a modified bolus on/off scheme (two days off, one day on).

CHAPTER 4 PAPER II: COMPENSATOR-BASED INTENSITY-MODULATED RADIATION THERAPY FOR MALIGNANT PLEURAL MESOTHELIOMA POST-EXTRAPLEURAL PNEUMONECTOMY

This chapter investigates the potential of compensator-based intensity-modulated radiation therapy (CB-IMRT) as an alternative to multileaf collimator (MLC)–based intensity-modulated radiation therapy (IMRT) to treat malignant pleural mesothelioma (MPM) post-extrapleural pneumonectomy. This study points out the challenges in planning and delivery of large fields on a specific linear accelerator with MLC. The study focuses on producing dosimetrically acceptable and deliverable IMRT plans for treating large modulated fields with solid modulator and step and shoot MLC. These plans are also calculated on a phantom for the quality assurance test of absolute point dose and relative dose distributions.

(J Appl Clin Med Phys. 2008 Oct. 29; 9(4): 98-109)

4.1 Synopsis

Treatment plans for four right-sided and one left-sided MPM post-surgery cases were generated using a commercial treatment planning system, XIO/CMS (Computerized Medical Systems, St. Louis, MO). We used a 7-gantry-angle arrangement with 6MV beams to generate these plans. The maximum required field size was 30x40 cm^2. We

evaluated IMRT plans with brass compensators (●Decimal, Sanford, FL) by examining isodose distributions, dose–volume histograms, metrics to quantify conformal plan quality, and homogeneity. Quality assurance was performed for one of the compensator plans.

Conformal dose distributions were achieved with CB-IMRT for all 5 cases, the average planning target volume (PTV) coverage being 95.1% of the PTV volume receiving the full prescription dose. The average lung V_{20} (volume of lung receiving 20 Gy) was 1.8%, the mean lung dose was 6.7 Gy, and the average contralateral kidney V_{15} was 0.6%. The average liver dose V_{30} was 34.0% for the right-sided cases and 10% for the left-sided case. The average number of monitor units (MUs) per fraction was 980 MU for the 45-Gy prescriptions (mean: 50 Gy) and 1083 MU for the 50-Gy prescriptions (mean: 54 Gy).

Post-surgery, CB-IMRT for MPM is a feasible IMRT technique treated with a single isocenter. Compensator plans achieved dose objectives and were safely delivered on a Siemens Oncor machine (Siemens Medical Solutions, Malvern, PA). These plans showed acceptably conformal dose distributions confirmed by multiple measurement techniques. Not all linear accelerators can deliver large-field MLC-based IMRT, but most can deliver a maximum conformal field of 40x40 cm^2. It is possible and reasonable to deliver IMRT with compensators for fields this size with most conventional linear accelerators.

The future work will address the skin dose of compensator-based IMRT treatments.

Key words: malignant pleural mesothelioma, compensator-based IMRT, SMLC IMRT, plan conformality, quality assurance

4.2 Introduction

Treating malignant pleural mesothelioma (MPM) post-surgery requires very large fields. This paper addresses intensity-modulated radiation therapy (IMRT) plans with solid modulators for the large fields required to treat MPM post-surgery, given that these plans first closely achieved the prescription dose objectives, passed the quality assurance (QA), and were safely delivered.

Malignant pleural mesothelioma is a fatal aggressive cancer of the pleura and a large complex target volume. Reports show that the incidence of the disease is increasing globally, with 2000 new cases annually in the United States[38]. Increased incidence of mesothelioma is strongly associated with exposure to asbestos, which is most commonly used in Western industrial societies; more men than women are affected[39]. In 2003, the Surveillance, Epidemiology, and End Results Program of the U.S. National Cancer Institute projected the total number of MPM cases in American men to be approximately 71,000 by the year 2054[40]. Because of the predicted numbers of new cases, the National Cancer Institute is sponsoring clinical trials designed to seek new treatment modalities.

Traditionally, radiation therapy treatment techniques used external beam radiation with a combination of photon and electron beams[41, 42] and intraoperative brachytherapy with post-operative mixed photon irradiation[43]. Normal tissue was spared using photon and electron blocks for external beam treatments. Various dose regimens have been prescribed for palliation and local control of this disease, ranging from 30 Gy[44] to a median dose of 36 Gy[45] (palliation) and 54 Gy (45 – 54 Gy, local control)[46] administered to the hemithorax. The latter treatment showed improved local control with acceptable toxicity. This finding seems to demonstrate that a sufficient dose was achieved for palliation and local control of the disease with the conventional techniques. Published literature lacks metrics, including dose–volume histograms (DVHs), which have increasingly become a crucial part of plan review, and comparisons complementing isodose distribution in transverse and orthogonal planes. Radiation oncologists often use information from computed tomography (CT), magnetic resonance, and positron-emission tomography imaging to accurately delineate the target and organs-at-risk (OAR) volumes so as to prescribe and quantify the dose to these sensitive overlapping structures. The use of IMRT allowed for further dose escalation to large target volumes while maintaining tolerance doses to abutting radiation-sensitive structures[47]. Post-operative IMRT for MPM has shown the most promising early local control of this disease[48-50]. Current techniques often couple IMRT from a specific treatment planning system with specific beam delivery and verify systems. Stevens et al[67] found that Corvus, Pinnacle, and Eclipse treatment planning systems were all capable of generating acceptable IMRT plans for MPM after extrapleural pneumonectomy (EPP). The authors compared treatment planning systems and found that the early plans with Corvus had the largest

number of monitor units (2786 MUs) and segments (1050 segments), and that a newer version of Eclipse had the least number of MUs (1813 MUs) and segments (173 segments).

Delivery of large IMRT fields with a multileaf collimator (MLC) is limited by MLC designs[51]. For example, the Siemens Oncor machine (Siemens Medical Solutions, Malvern, PA) with 82-leaf Optifocus MLC system allows for a maximum IMRT field size of 22x40 cm^2. The MLC carriage-over-travel distance past the central axis is limited to 10 cm. Even though a field size of 24x40 cm^2 can be accommodated, given that the smallest segment size can be set to 2x2 cm^2, larger IMRT field widths are required to treat MPM. To overcome the MLC field size limitations, treatments with multiple isocenters have been proposed by other investigators[19]. We investigated a compensator-based IMRT (CB-IMRT) technique with a single isocenter to treat MPM post-surgery.

It is essential that the modulator (MLC or solid brass compensator) reproduce the intended fluence map. For three of four right-sided cases, a number of IMRT fields required a minimum field width of 26 cm. These cases were good candidates for CB-IMRT delivery (which has no IMRT field size limit, and for which a maximum conformal field size of up to 40x40 cm^2 is possible) on the Siemens Oncor machine. Intensity-modulated radiation therapy with compensators has been successfully used for more than a decade[52,53]. The CB-IMRT technique offers continuous intensity modulation. Compensators deliver the intensity-modulated dose in static form to all

57

points within a field relatively instantaneously where the beam-on time depends on the machine dose rate.

To investigate the potential of very large field CB-IMRT for MPM, the goal was to create plans that closely achieved the prescription dose objectives for MPM post-surgery and that produced manageable modulators that were delivered on our Siemens Oncor treatment machine.

4.3 Materials and Methods

All data sets acquired for this test study came from patients who underwent surgery before simulation.

4.3.1 Surgery

The EPP procedure involves removal of the ipsilateral lung (remove motion) and hemi-diaphragm resection, with subsequent reconstruction using polytetrafluoroethylene fabric. A mediastinal lymph nodes dissection is also performed, as is a chest wall resection and reconstruction. To assist the radiation oncologist with the contouring, the surgeons place clips to identify the entire outline of the resected hemi-diaphragm and the resected margins. These areas are otherwise difficult to identify post-operatively. The simulation for treatment planning occurs 6 – 8 weeks post-surgery.

4.3.2 Simulation

Surgical scars were typically wired and then covered with bolus (7 cm wide, 0.50 cm thick) extended 4 cm proximally and distally over the scar. Patients were immobilized supine on the CT couch using a wing board (Med-Tec, Orange City, IA) in combination with a vacuum bag and the T-bar system indexed to the couch top. The T-bar helps support the arms up and out of the radiation field. Radio-opaque ball bearing markers were taped to the anterior and lateral sides of the patient for treatment planning and as a setup reference.

Simulation CT slice thicknesses were typically 5 mm (no larger). At least 100 transverse slices were acquired and transferred to the treatment planning system.

4.3.3 Contours

The use of IMRT required contouring of the clinical target volumes (CTVs), which included the tumor bed (post EPP) and the regions at risk for seeding of disease. The CTV extended from T1–L3 (from apex of thorax to inferior pole of kidney). The contours for the contralateral lung, kidneys, heart, liver, esophagus, small intestine, spinal cord, and skin were drawn on every slice (a time-consuming process). The three dimensional auto margin functions were used to create a PTV0.5 cord (CTV + 0.5 cm) and cord avoidance (cord + 0.5 cm) structure. Avoidance and boost structures were drawn manually. To account for uncertainties in contouring the CTV, superior and inferior

margins were set 1 cm above and 1 cm below the most superior and most inferior surgical clips. The anterior, posterior, and lateral margins were defined by adding 0.75 cm to violated spaces clipped at the skin.

4.3.4 Treatment Planning

Coplanar IMRT beams (6MV) aimed at the center of the planning target volume (PTV) were designed. The first gantry angle was 180 degrees, and the remaining 6 angles were at about 30- to 45-degree intervals, excluding the anterior–posterior field. These were selected using a beam's eye view tool to minimize entrance and limit exit doses to contralateral lung. Gantry angles were adjusted as much as possible while obtaining the desired dose distributions. We noticed that liver position varied in the superior–inferior direction with respect to CTV position for these cases. Planning right-sided cases with sufficient CTV coverage, given the extent of liver in the radiation field, was more challenging because of the competing dose constraints of these structures.

4.3.5 IMRT Plans

Seven fields (gantry angles), A – G, were selected to conform to PTV using MLC. Fields A – D were split to keep the compensator weights manageable, resulting in additional fields A1 – D1. Fields A and A1 were split in the inferior–superior direction with at least a 2 cm overlap margin. The PTV contour seen by each field was also edited and MLC conformed to the new split contour shapes. The same procedure was repeated for fields

that needed to be split. The fields were split at varying distances from central axis to help reduce possible high dose at the junction area.

4.3.6 IMRT Prescription Page

Target and OARs were set up in the IMRT prescription page according to the prescription guidelines shown in Table 3. Deviation from goal doses for the minimum and the maximum PTV coverage was given the highest penalties. Liver, kidneys, contralateral lung, and heart were given higher overlap priorities than were the other OARs. Maximum dose to the liver was set to the maximum PTV dose with relaxed penalty, but certain percentages of liver and contralateral lung volumes were restricted to very low doses with very high penalties. The point was to achieve the suggested prescription dose objectives to these structures.

Table 3. Dose–volume guidelines for the target and organs at risk (OARs)[a].

Target or OAR	Dose–volume guideline
Clinical target volume	$V_{100} > 98\%$
Planning target volume	$V_{100} > 95\%$
Contralateral lung	$V_{20} < 4\%$
Mean lung dose	6–8 Gy or ALARA
Spinal cord	Less than 10% > 45 Gy
	0.0% > 50 Gy
Heart	$V_{45} < 50\%$
Liver	$V_{30} < 30\%$ or ALARA
Right kidney	$V_{15} < 20\%$
Left kidney	$V_{15} < 20\%$
Esophagus	$V_{55} < 30\%$

[a,] The planning target volume is the clinical target volume plus 0.5 cm. The V_{100} is the volume receiving 100% of the prescribed dose. Contralateral lung V_{20} is the volume of lung receiving 20 Gy. Lung mean lung dose and liver V_{30} are kept as low as reasonably achievable (ALARA).

4.3.7 Compensator Plans

4.3.8 Treatment Planning Strategy

Our CB-IMRT plan strategy process started with an arrangement of 5 non-coplanar fields for the left-sided case and arrangements of 7 coplanar fields for the right-sided cases, which resulted in acceptable dose distributions but very heavy modulators (weight up to 15.9 kg). An 11.3-kg compensator from the 7-field arrangement is shown in Figure 19. These large fields were then split, which resulted in 7-gantry 14-coplanar fields with field junction overlap matched at the central axis, using modulators 7.62 cm thick that yielded acceptable dose distributions with 125% hot spots in the junction area. The average

compensator weight was 8.2 kg (range: 6.3 – 9.1 kg). We did not achieve the plan objectives if all beams were modulated with the brass modulators (5.08 cm maximum thickness), even with the MLC blocking. The outcome was a 7-gantry 11-coplanar field arrangement with modulators (5.08 cm and 7.62 cm maximum thickness) and field junction overlap at varying distance from the central axis. The median compensator weight was 7.5 kg (5.2 – 10.0 kg).

All CB-IMRT plans were generated using an MLC blocking that conformed the beam to the PTV plus a 0.5 cm block margin. We found it desirable to plan the compensator fields with MLC blocking advantages. In addition, individual MLC leaves can be edited to further enhance the distribution even after the compensators are generated. The effective attenuation coefficient (EAC) values were assigned for all fields. We used compensators (7.62 cm maximum thickness) with an intensity modulation range of 8% – 100% for fields that contained significant parts of the contralateral lung or liver. These large fields would produce heavy modulators, and thus were divided. We used compensators (5.08 cm maximum thickness) with an intensity modulation range of 20% – 100% for fields that contained no significant parts of lung or liver. The only lung had to be spared. We tried to keep the 10-Gy isodose line outside the contralateral lung and kidney volumes to maintain prescription guidelines to these structures. All IMRT plans were calculated using superposition with heterogeneity corrections applied.

Dose distributions and DVHs were reviewed by the radiation oncologist. Each field was set up in the IMPAC Record and Verify system (IMPAC Medical Systems, Sunnyvale,

CA) with its unique accessory tray code (S2N01–S2N18). Two coded trays are shown in Figure 19. Compensator thickness files were electronically sent to ●Decimal for fabrication; the modulators were returned within 24 hours.
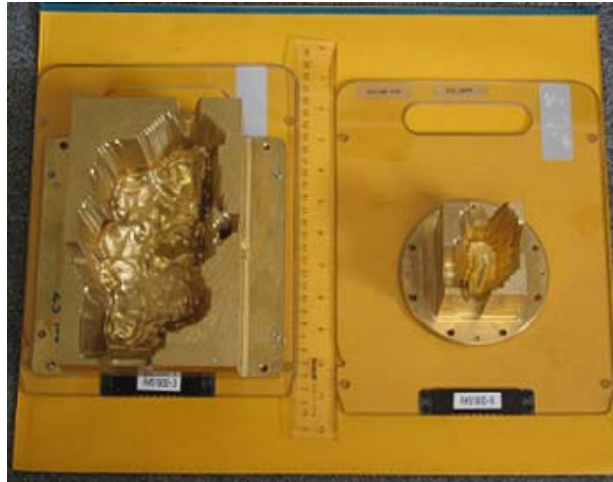
Figure 19. Two modulators from ●Decimal mounted on the Siemens coded trays. One of the large compensators (11.3 kg) from the initial 7-field plan that did not require extensive blocking within the field is shown next to one of the 7-field IMRT modulators for prostate (1.8 kg).

4.3.9 Compensator Thickness File

The brass thickness **t** (**i,j**) can be calculated as a simple exponential attenuation equation for an array of values each representing the filter thickness for each ray line at (**i**, **j**) as in equation 2:

$$t(i, j) = -\frac{\ln[trans(i, j)]}{\mu_{eff}} \qquad (2)$$

where Trans($\mathbf{i}$, $\mathbf{j}$) is the transmission for each ray line throughout the compensator and μ_{eff} is the EAC for solid brass compensator under broad-beam geometry. du Plessis et al.[54] showed that the absorbed dose varies exponentially as a function of absorber thickness on the beam axis at any depth in water for any material. These authors showed that EAC for brass can vary by as much as 13% over a depth range of 4 – 39 cm. The measurement showed that EAC values decreased with increasing field size, depth, and thickness as beam hardening and more scatter for larger field sizes contributed to dose at the given depth.

Beam divergence and beam hardening is taken into account by the treatment planning system dose computation. Mean energy of the beam increases after the beam passes through the modulator. Jiang and Ayyangar[55] showed that beam hardening resulted in greater change (sparing) in surface dose than in dose at depth with respect to maximum dose. Authors showed that for a 6MV 10x10 cm^2 beam, a 10% maximum dose reduction occurred in surface dose and a 3% dose increase occurred in percent depth dose at 10 cm depth for Cerrobend slab 5 cm thick ($\mathbf{p}$ = 9.76 g/cm^3).

4.4 Safety Considerations

We considered limiting the maximum compensator weight to a level that therapists were comfortable with in safely handling the device. We had the therapists try the 10 kg and 15.9 kg compensators. The therapists who could easily handle the 45-degree solid wedge (which is 6.1 kg) were able to insert the 10 kg modulators into the wedge slot with ease;

the 15.9 kg modulators posed more of challenge for most of the therapists. The manufacturer's recommended weight limit for the Siemens Oncor block tray accessory is 15.9 kg; however, we do not have the weight limit information for the wedge tray slot accessory. We tried to exercise safety in handling the relatively heavy modulators.

Modulators were loaded with the gantry set at 90 degrees or 270 degrees. The delivery was such that no loaded compensator field crossed over the patient at any time, and for patient safety, plans were designed without the anterior–posterior field.

4.4.1 Plan Evaluation

We used two-dimensional isodose distributions (axial, sagittal, and coronal planes) to visually inspect the target coverage. Quantitative techniques such as DVH analysis and other indices were used to evaluate the plans. Table 4 shows the fraction of PTV volume receiving 100% of the prescribed dose in grays (PTV V_{100}); high dose in grays to 5% of PTV volume (PTV D_{05}); conformation number (CN), an index proposed by van't Riet et al.[56] , which takes into account the quality of coverage of the target and the volume of healthy tissue receiving at least the prescribed dose; and the homogeneity index (HI) as the ratio between maximum dose and prescription dose within the target. In addition, contralateral lung V_{20}, V_5, and mean lung dose (MLD); V_{30} for liver; V_{45} and V_{50} for heart; V_{15} for contralateral kidney; and maximum cord dose and dose to 10% of cord (D_{10}) were used to score OAR protection. Treatment efficacy with compensators in terms

of MUs per field, total MUs, and beam-on time per daily fraction and per total treatment time are reported.

4.4.2 Quality Assurance

We used multiple measurement techniques to perform IMRT QA. Dose distributions for one of the compensator plans were recalculated for three QA phantoms. This repetition provided the reference for comparison with absolute point dosimetry measurement using a calibrated ion chamber, single coronal field using absolute dose distributions measurement with the Map Check diode array device (Sun Nuclear Corporation, Melbourne, FL), and composite dose distributions at 4 transverse film planes irradiated simultaneously with true gantry angles incident on the phantom. We registered extended dose range (EDR2) films to the plan and analyzed them using the RIT 113 film dosimetry system (RIT Inc., Denver, CO).

4.5 Results

Figure 14 (a–d) shows isodose distributions for right-sided and left-sided cases. Notice that the 10-Gy isodose line is kept outside the contralateral lung. Figure 14 (a,b) shows dose distributions in the coronal and sagittal planes, and dose profile at various distances from the central axis in those planes. Figure 14 (a) shows the coronal dose distributions for the right-sided case. The flat dose profiles show that dose varies 2% across the coronal plane and 6% along the plane. Figure 14 (b) shows the dose distributions for the

right-sided case in the sagittal plane. The profile throughout the field junction shows 118% hot spots. Figure 14 (c) shows the 50-Gy prescription dose distributions for the right-sided case. Figure 14 (d) shows the dose distributions for the left-sided case. Figure 15 (a,b) shows DVHs for one of the right-sided and the left-sided MPM case.

(a)(b)

(c)(d)
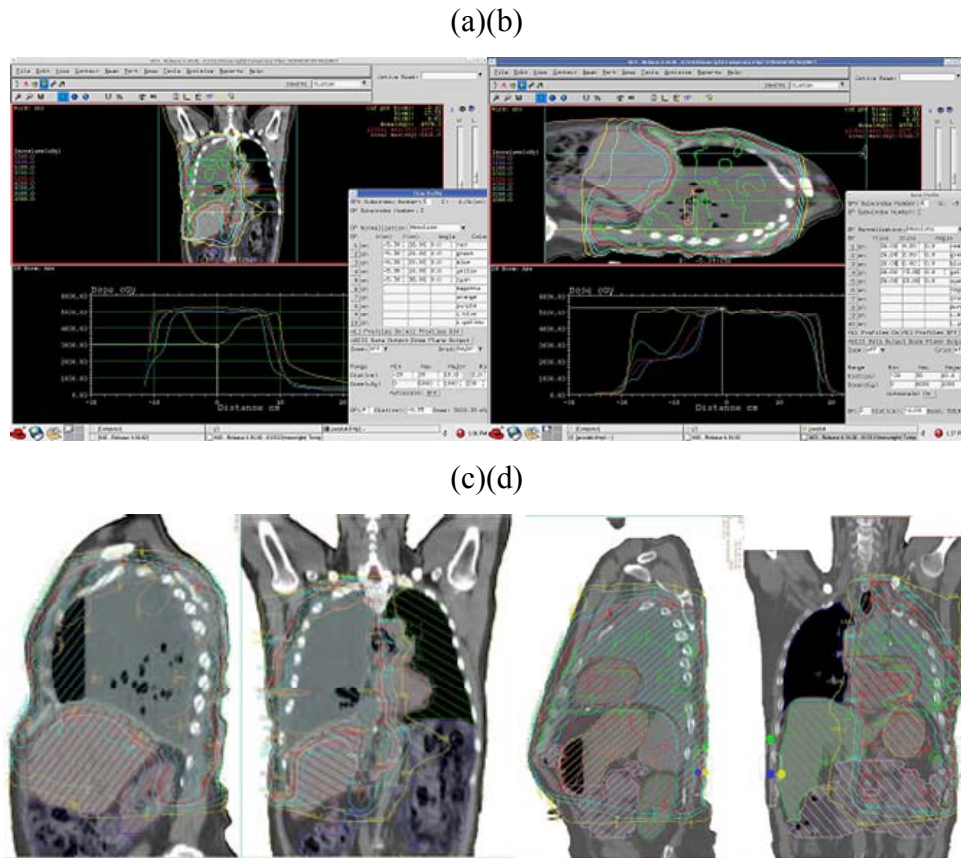
Figure 20. Dose distributions and profiles in the coronal and sagittal planes. (a) Sagittal profile of a right-sided case shows the profiles across the coronal plane at isocenter, ±2 cm from isocenter, and 6 cm inferior and 12 cm superior to isocenter. The profile 6 cm inferior to isocenter shows the degree of liver-sparing in this plane. (b) Coronal profile of a right-sided case shows the profiles at isocenter, ± 2 cm from isocenter, and 5 cm posterior and 8 cm anterior to isocenter plane. (d) Dose distribution for the left-sided case is shown.

All plans conformed to 99.2% of CTV volume and 95.5% of PTV volume achieving the prescription dose. Lung V_{20} was less than 2%, and MLD ranged between 5 Gy and 8 Gy for all plans. All lung MLDs and V_5s were below the range at which pneumonitis was no longer reported to have been observed by other investigators[57]. The average value for liver V_{30} was 34%.

To compare IMRT treatment parameters with segmented MLC (SMLC) and compensator delivery on the Siemens machine, we used the same field configuration in planning 2 cases with SMLC IMRT. Large optimized fluence had to be segmented with a minimum MLC segment size greater than 2 cm^2 (because of IMRT field size limitations) to produce deliverable plans. More desirable and better dose delivery resolution was not possible in this case. In Table 4, note that (TV_{RI}/V_{RI}) is worst for plan 5 with MLC (5LM). As compared with compensator plan 5LC, this plan shows more non-target tissue receiving the prescription dose.

(a)
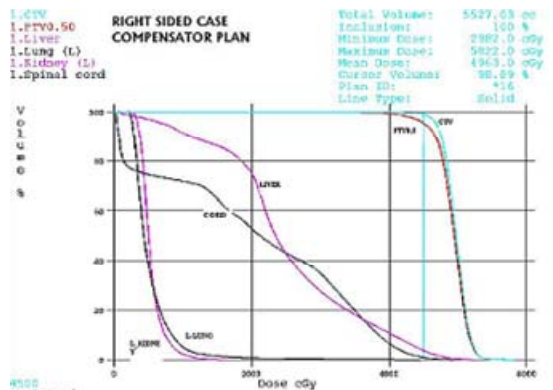
(b)
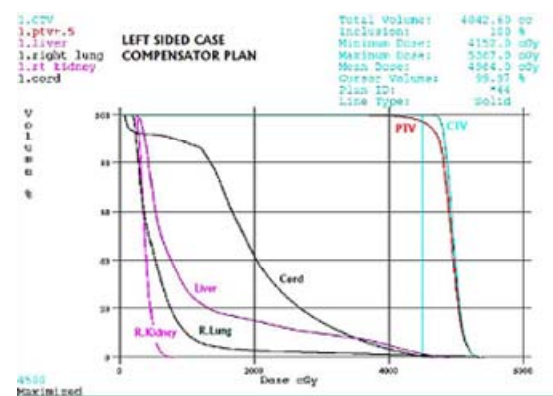
Figure 21. Dose–volume histograms for the planning target volume (PTV), clinical target volume (CTV), and the liver, lung, kidneys, and spinal cord for (a) a right-sided case, and (b) the left-sided case.

One possible explanation may be that plan 5LM needed to have a smaller segment size, and thus higher dose sculpting power, to block portions that needed to receive less dose. This plan also had higher HI than did the compensator plan. Table 4 also shows MLC parameters such as total number of segments and MUs, and total treatment time. Total number of MUs was 1993 MUs with 244 segments for plan 1RM (Table 4). Treatment time per beam can be seen to be significantly shorter for compensators. The total number

of MUs was doubled for SMLC. Total treatment time was slightly shorter for compensator delivery, and yet comparable with automated SMLC delivery as shown in Table 3.

Table 3 shows the number of MUs for the 5 compensator and 2 MLC plans. Our plans for 4 right-sided and 1 left-sided case resulted in an average of 980 MU (range: 882 – 1040 MU) per daily fraction. The average daily delivery time was 33 minutes, which included entering the room to check the isocenter and to replace the compensators for all fields.

Table 4. Plan values[a].

Plan ID	PTV V_{100} (%)	PTV D_{05} (Gy)	(TV_{RI}/TV)	(TV_{RI}/V_{RI})	CN	HI
1RC	95	52	0.95	0.96	0.92	1.3
1RM	95	55	0.95	0.96	0.91	1.4
2RC	95	54	0.95	0.82	0.78	1.5
3RC	95	54	0.95	0.90	0.86	1.2
4RC	95	56	0.95	0.93	0.88	1.2
5LC	97	52	0.97	0.85	0.83	1.2
5LM	98	55	0.98	0.81	0.80	1.5

[a.]Plan 1RC (plan 1, right-sided case, with compensators) shows that 95% of the planning target volume (PTV) received 100% (V_{100}) of the prescribed dose of 45 Gy. The high dose to 5% of the PTV volume is 52 Gy for the compensator plan and 55 Gy for the multileaf collimator (MLC) plan 1RM (plan1, right-sided case, with MLC).
PTV = planning target volume; TV = target volume; RI = reference isodose line; CN = conformation number; HI = homogeneity index; V_{100} = volume receiving 100% of the prescribed dose; D_{05} = high dose to 5% of the volume; plan ID key: plan number (1 – 5), right- or left-sided (R, L), compensator or multileaf collimator (C, M).

Table 5. Plan delivery values[a].

Plan ID	Average MUs per field	Total MUs	Segments	Average beam-on time per field (s)	Total treatment time (min)
1RC	89	976	—	18	33
1RC[b]	98	1083	—	23	34
1RM	181	1993	244	198	36
2RC	87	962	—	18	33
3RC	94	1040	—	19	35
4RC	97	1039	—	19	35
Avg. RC	92	1004	—	18.5	34
5LC	80	882	—	16	30
5LM	164	1801	193	126	35

[a.] The average beam-on time per field for compensator plans 1RC – 4RC and 5LC was calculated based on 300 cGy/MU at the central axis. The number of segments are shown for the multileaf collimator plans 1RM and 5LM. Total treatment time for compensator delivery includes entering the treatment room to replace the compensator for each field. Plan ID key: plan number (1 – 5), right- or left-sided (R, L), compensator or multileaf collimator (C, M).
[b.] For 50 Gy prescription dose.

4.5.1 QA Results

The measured absolute dose in water and in cube phantom for the composite plan agreed within 3% of the calculated dose. Figure 16 (a) shows one of the individual fluence maps from Map Check. At least 95% of the measured and calculated isodose distributions were found to be in agreement within 3% and 3 mm distance to agreement for all individual compensator fields. The large EDR2 film dosimetry showed 117% hot spots in the junction area, consistent with the predicted value. Figure 16 (b) shows the QA results

using the cube phantom. The measured orthogonal profiles were extracted, which showed

good agreement with the calculated profiles.

(a)
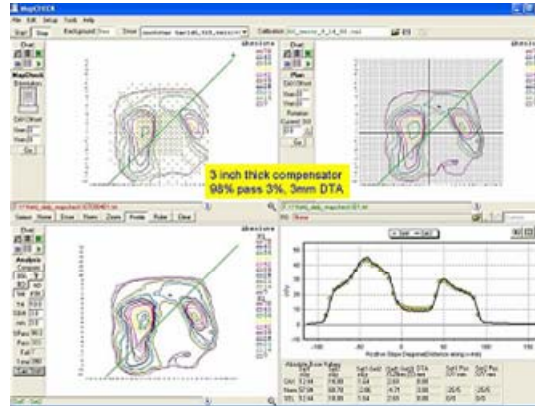
(b)
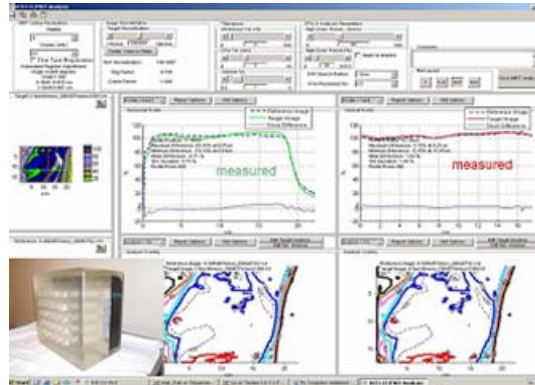
Figure 22. The calculated and measured isodose distributions in the coronal plane for one of the compensator fields is shown in the top right and top left quadrants. At the bottom left, the overlaid absolute dose distributions are seen. Overlaid oblique profiles are shown in the bottom right quadrant. DTA = distance to agreement. (b) The cube phantom is shown at the lower left. The RIT film dosimetry system (RIT Inc., Denver, CO) analysis window shows good agreement between the measured and calculated dose distribution.

4.6 Discussion

Although the words "compensator" and "solid modulator" were used interchangeably throughout this chapter, the intention was to refer to the same device that modifies the intensity of the beam. The goal of the present study was to devise a CB-IMRT technique for MPM post-surgery that met the prescription objectives and could be safely delivered. The results reported here are based on the reference dose of 45 Gy. We also tested the technique for a higher prescription dose. We found that the results also apply to the prescription dose of 50 Gy. We re-optimized plan 1RC (plan1, right-sided case, with compensators) for a higher prescription dose of 50 Gy. Figure 14 (c) shows the dose distribution. We achieved the prescription objectives with at least 95% of the PTV volume receiving 50 Gy, with a mean dose of 54 Gy. Liver V_{30} was less than 36%, contralateral lung MLD and V_{20} were 5.7 Gy and 1% respectively. No portion of cord received 50 Gy. The total number of MUs for the 50-Gy plan for the right-sided case was 1083 MU.

We used conformity number as one of the metrics to quantify conformal plan quality. The conformity number is defined in equation 3. We calculated the DVHs for all tissue and non-tissue (unspecified tissue not contoured). The target volume covered by the reference isodose line, TV_{RI}, was calculated. The first term in equation 3 takes account only of quality of target coverage. This value for right-sided plans was 0.95 for compensator plans (as in Table 4). The second term describes the ratio of the PTV volume that received the prescription dose to the volume of the reference isodose line.

All non-target tissue and non-tissue volume covered by the reference isodose line was summed. The average value for the 4 right-sided cases was 0.90 for compensator plans and 7.2% of non-target tissue for right-sided cases. For left-sided case with compensators, 12.3% received the prescription dose. If the CN value is 1, the target conformity is 100% and the dose must fall rapidly outside the large PTV. As indicated earlier, part of the liver and kidney volumes fell inside the PTV because of overlap. In fact, about 10% of liver volume received the reference dose.

$$CN = (\frac{TV_{RI}}{TV}) * (\frac{TV_{RI}}{V_{RI}})$$
(3)

4.7 Conclusions

We found that CB-IMRT with 7 gantry angles produced dosimetrically acceptable plans for a single isocenter, without the need to match electron fields; however, it produced heavy modulators. The same gantry angles with 11 coplanar 6MV IMRT fields produced acceptable conformal plans and closely achieved the prescription dose objectives. The resulting modulators with an equivalent field size of 26 cm^2 were easier to manage. Total treatment time for manual CB-IMRT delivery was comparable with automated SMLC delivery. For MPM, CB-IMRT showed acceptably conformal dose distributions confirmed by multiple measurement techniques. Not all linear accelerators can deliver large-field SMLC-based IMRT with a single isocenter, but most can deliver a maximum conformal field size up to 40x40 cm^2. It is possible and reasonable to deliver IMRT with compensators for fields this size with most conventional linear accelerators. IMRT with

solid modulators adds an additional option to existing linear accelerators (LINACs) to treat large target volumes, as was the case for MPM post EPP.

CHAPTER 5 PAPER III: 6MV BUILDUP DOSE FOR COMPENSATOR-BASED IMRT COMPARED TO MLC-BASED IMRT

Dose in the buildup region was investigated for intensity-modulated radiation therapy (IMRT) delivery with solid brass modulator and MLC. A Varian Clinac 2100 linear accelerator (LINAC) with MLC was used for beam delivery. A solid brass step jig was designed and built to conduct IMRT test with compensator. Two step and shoot sequences were programmed to conduct IMRT test delivery with MLC. The profiles of the two delivery techniques were measured and adjusted to match at isocenter depth of 10 cm. Buildup dose at 1-5 mm depth was measured with an ultra-thin fixed volume parallel plate ionization chamber. Monte Carlo was used to model the brass step jig and step and shoot MLC sequences. The measured and simulated profiles for the two IMRT techniques were matched at isocenter depth of 10 cm. Component doses including MLC component dose was calculated. Mean spectral energy for open beam and compensated beam was calculated.

(Intend to submit)

5.1 Synopsis

Dose in the buildup region of a 6MV Varian LINAC was compared for IMRT delivery with solid modulators and MLC. Near skin buildup dose of compensator treatment was a concern since compensator was closer to skin for Varian LINAC compared to existing machine. Dose was measured for 90 cm source to surface distance (SSD) and 106 cm SSD. The buildup depth was 1, 3, and 5 mm. Component doses including MLC component dose was calculated. Mean spectral energy was calculated for compensator. Buildup dose variation with SSD, field size and beam incidence angle was calculated. The agreement between the measured and calculated IMRT profiles for compensator and MLC was ±1.5 %.

Key Words: Buildup dose, IMRT, step Jig, Monte Carlo, compensator, MLC

5.2 Introduction

Dose in the buildup region has been an area of interest in clinical radiation therapy even before 3D conformal therapy was introduced[58]. The modeling of the dose in the buildup region when using intensity-modulated radiation therapy (IMRT) treatments has been the subject of radiation physics research since the use of IMRT for head and neck cancer[59]. Excessive dose in the buildup region can be the cause of significant patient discomfort and may lead to treatment interruptions, while underdosing in the buildup region may result in a local failure. Most commercial planning does not model dose in the buildup

region well for small fields, such as the ones used in IMRT, and may not model the dose well with brass filters in the beam path.

Many factors contribute to buildup dose, including the photon beam energy spectrum, scattered or contaminant electrons and their angular distribution, and scattered low energy photons. Traditionally, these quantities are not modeled well in commercial treatment planning systems. As a result of this deficiency, current commercial treatment planning systems have difficulties in calculating dose in buildup regions, as reported by Chung, et al.[60]. These authors found that two TPS overestimated surface dose by 7.4% to 18.5%. The dosimetrical differences in buildup regions between different treatment modalities, such as MLC-based versus compensator-based IMRT, cannot be accurately obtained by comparing treatment plans.

IMRT[61] planning uses inverse planning algorithms[62] that generate idealized fluence maps for each field. The fluence maps then must be converted to either a series of MLC segments that are deliverable. There are two techniques for using the MLC to deliver the fluence maps: step and shoot, and sliding window. In the step and shoot approach, each segment is formed, then the beam is turned on for the appropriate number of monitor units (units of delivered radiation). Then the beam is held off and the next segment is formed, and the process repeats. In the sliding window approach, slits of variable width move across the field and the dose rate is modulated.

The fluence map for each field can also be made deliverable using custom compensators. The desired fluence is sent to a computer controlled milling machine, which is used to mill out a solid brass plug to form a custom compensator for each field. The intensity is modulated by continuously varying the brass thickness. For each field, the associated compensator is placed in the beam path, typically in the wedge slot. Unlike the step and shoot delivery technique where only parts of the field are exposed to radiation at a time, the entire field is exposed in a static fashion.

Another major difference between the two IMRT techniques is that the compensator is always mounted closer to the patient than MLC is. This geometric difference could change the dose in the buildup region. This geometry difference is largely due to accelerator design. Of the different LINAC designs, the Varian LINACs mount puts the compensators closest to the patient and early studies in MLC scatter and block scatter have shown that the closer the aperature, or in this case the compensator, the more scatter reaches the buildup region. However, compensators also filter out low energy photons and eliminate low energy electrons that are scattered from the LINACs collimation system.

Measuring dose in the buildup region is by itself an area of research. There is an absence of electron equilibrium and the finite size of the fixed volume ionization chamber creates an uncertainty as to the exact dose and the exact point of measurement. Although the extrapolation chamber, which allows one to vary the chamber volume, is the detector of

choice for buildup dose measurements, this device is bulky, time consuming to use, and is not available in many clinical settings, perhaps due to its limited use.

Fixed volume parallel plate ionization chambers are widely used to measure superficial dose. Velkley et al[63] proposed corrections to reduce the over-response of these chambers. The known over-response of these chambers at the surface has been compared with the extrapolation chamber and LIF thermo luminescent detectors and the authors proposed guidelines in use of such detectors[64]. Chamber specific correction factors have been reported by others (Rawlinson et al)[65]. Rawlinson modified Velkley's correction factor for fixed volume parallel plate ionization chambers to include chamber geometry and wall material density. This correction factor was used in this study.

Buildup dose was investigated for MLC-based IMRT and compensator-based IMRT delivery with a Varian (Varian Medical System Inc. Palo Alto, CA) linear accelerator (LINAC). To understand the differences in buildup doses between the delivery techniques, we commissioned a Monte Carlo code to calculate the buildup dose and component dose by components. So the MLC scatter dose photons, electrons and the scatter from the compensator were all individually evaluated. In addition, the mean spectral energy for compensators was calculated. Finally, the total doses and component doses were compared for the two delivery techniques.

81

5.3 Material and Methods

5.3.1 Study Setup

A brass step modulator was designed and built to deliver a simple IMRT profile for a single field using a 6MV beam on a Varian 2100. The simple design would allow for relatively straightforward modeling of the resulting dose with Monte Carlo. To create a similar profile at 10 cm depth, using an MLC to modulate the beam, a series of equivalent MLC steps were also created for step and shoot delivery with Varian Millennium MLC. A commercial linear diode array (Sun Nuclear Profiler, Sun Nuclear Corporation, Melbourne, FL) was set up to measure profiles of compensator and MLC steps at isocenter depth of 10 cm. By adjusting the index of the MLC segments and adjusting the MLC shapes slightly, the MLC profiles were then matched to the profile of the brass compensator. Doses at a variety of depths in the buildup region were measured in solid water using an ultra-thin fixed volume parallel plate ionization chamber connected to an electrometer.

The MLC sequences and the brass modulator were modeled with Monte Carlo. The simulated parameters for the MLC and brass steps were adjusted to match their profiles to corresponding measured profiles at 10 cm depth.

5.3.2 Solid Brass Modulator

The modulator is a 21x15 cm^2 solid brass step as shown in Figure 23. It is mounted on an open port Plexiglas tray and inserted into the head of the machine so that the proximal surface of the compensator is 57.6 cm from the source or 42.4 cm from the phantom surface. The distance from the distal surface of the compensator to the phantom surface varies from 41.8 to 35.4 (for 7 cm brass).
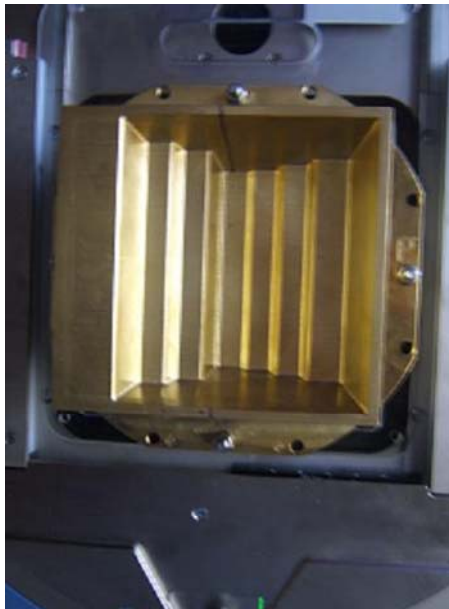
Figure 23. Brass modulator mounted on an open port Plexiglas tray inserted into upper wedge slot of LINAC. From left to right side of the figure, the step thickness is 7.62, 5.08, 4.0, 0.6, 1.0, 2.0 and 3 cm. Step width varied from 2.5 to 3.4 cm projected at the isocenter. The effective Jaw setting was 21.4x15.4 cm^2 at this plane.

5.3.3 MLC Step and Shoot Sequences

Test fields were designed using the Varian MLC SHAPER program version 6.2. Because of the field width, a spilt field IMRT profile with seven step and shoot segments was designed to mimic the dose profile from the compensator at 10 cm depth.

The initial design of each segment used was 3x15 cm^2. The initial dose fraction values for each segment in a sequence, was estimated using equations 4 and 5. $BS1_i$ is the beam-on-time for segment i in sequence of the first field, and $BS2_i$ is the beam-on-time for segment i in sequence in the second field. For each MLC segment in sequence, the corresponding brass step thickness is x1i and x2i, μ (the effective linear attenuation coefficient) is 0.375 cm^{-1},

$$BS1_i = \frac{e^{-\mu x1i}}{\sum_{i=1}^{N} e^{-\mu x1i}} \tag{4}$$

$$BS2_i = \frac{e^{-\mu x2i_i}}{\sum_{i=1}^{N} e^{-\mu x2i}} \tag{5}$$

Weighted segment profiles were added to obtain the MLC step profile.

The segment weight $SW1_i$ and $SW2_i$ is calculated using equations 6 and 7:

$$SW1_i = BS1_i * \frac{MU1}{MU1 + MU2} \tag{6}$$

$$SW2i = BS2_i * \frac{MU2}{MU1 + MU2} \tag{7}$$

$MU1$ and $MU2$ are the monitor units set on the LINAC for sequence 1 and 2.

$$MU1 = \frac{\sum_{i=1}^{N} e^{-\mu x 1 i}}{\sum_{i=1}^{N} e^{-\mu x 1 i} + \sum_{i=1}^{N} e^{-\mu x 2 i}} \tag{8}$$

$$MU2 = \frac{\sum_{j=1}^{N} e^{-\mu x 2 i}}{\sum_{i=1}^{N} e^{-\mu x 1 i} + \sum_{i=1}^{N} e^{-\mu x 2 i}} \tag{9}$$

5.3.4 Matching Profiles at 10 cm Depth

Profiles of compensator steps and MLC segments were measured using a commercial linear diode array. The Profiler was set up so that the detector array was in a horizontal plane at 100 cm SSD (at isocenter), then 10 cm of solid water was placed on top of the Profiler. The profile generated from the compenator was carefully measured. The profile generated from the MLC delivery initially did not match. The leaf positions for the MLC delivery were adjusted until the gradients in the profile of the MLC delivery matched that of the compensator. Then the dose index for the MLC segments was adjusted to match the MLC profile to the compensator profile.

Finally the total number of monitor units was adjusted for the MLC delivery to deliver the same dose as the compensator plan. For this adjustment, an ion chamber replaced the Profiler in the phantom. In the end, 729 MUs (600+129) were delivered for the MLC sequences and 262 MUs for the compensator.

5.3.5 Chamber Measurements in the Buildup Region

An ultra-thin window (0.02724 mm) fixed volume parallel plate ionization chamber (EXRADIN model A10, with the same collector diameter and electrode gap as Markus chamber) was connected to a MAX 4000 electrometer (Standard Imaging, Demingway WI). The chamber was set up in plastic water at 90 cm SSD. Chamber readings (nC) were obtained in the buildup region for individual slabs as well as for all steps of the two IMRT delivery techniques. The entire step and shoot sequence was run to obtain chamber response for each step. The chamber readings were corrected using Velkley's correction factor which was modified by Rawlinson to account for geometry and wall material density, as in equation 10,

$$P'(d) = P(d) - C(E) * (\frac{1}{W}) * \rho^{0.8} e^{(\frac{-4d}{d\max})} \tag{10}$$

P'(d) is the corrected dose at depth *d*, *P(d)* is measured dose at *d*, the energy dependent factor *C(E)* is 27% for 6MV beam, *l* is plate separation, *W* is inner wall diameter, ρ is wall material density, *d* is the depth to front surface of chamber, and *d$_{max}$* is the depth of maximum dose respectively.

5.3.6 Monte Carlo Modeling

An EGSnrc[7]-based Monte Carlo simulation package for clinical radiation treatment units, BEAMnrc[34], was used to simulate the radiation from the Varian linear accelerator using either an MLC or brass compensators. The Varian Trilogy linear accelerator was first modeled for just open fields and tested against measured depth doses and dose profiles in a water phantom. Once this was completed a phase space file, in which are stored physical parameters (such as charge, energy, position, and direction) for all particles (photons and electrons) traversing the plane of interest, was scored below the secondary jaws. A total of 5×10^8 electrons with kinetic energy of approximately 6MeV incident on the target, were simulated to generate a phase space file. The phase space files were then used as radiation sources for MLC and compensator step simulations.

The phase space files from MLC and compensator step simulations were used as radiation sources in phantom dose distribution calculations using DOSXYZnrc[13] (DOSXYZ user's manual nrc report). In the DOSXYZ program the phantom geometry, compensator design, and, individual MLC profiles were defined. Water phantom simulations were done at 90 cm and 106 cm SSD. The buildup dose was calculated in components: the primary photon dose, the scattered radiation dose and electron contaminant dose. The energy fluence distribution for open beams and with a 2 cm thick slab of brass in the beam were calculated to show the effect of beam hardening with compensators.

The physical width and dimension of the brass steps were carefully measured and modeled using the component module BLOCK in which the compensator divergence was accounted for. For the MLC, each segment dimension was adjusted and simulated accordingly. The accelerator models are shown in Figure 24 (a, b). The weight for each MLC segment were defined by the monitor units delivered in each segment divided by the total number of MUs used to deliver the MLC pattern.
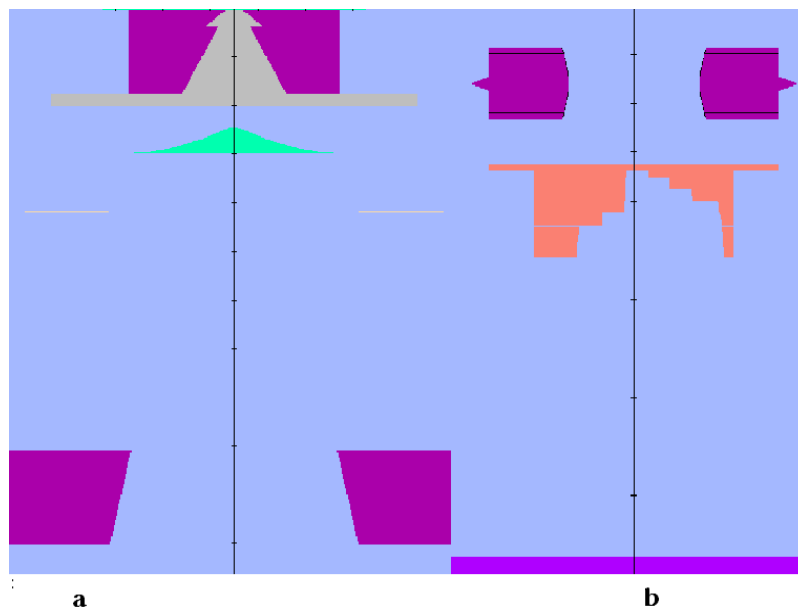
Figure 24. Monte Carlo model of Varian accelerator head geometry. Major parts such as the target, primary collimator, flattening filter, transmission chamber and jaws are shown in panel a. MLC, the step wedge and the phantom top is shown in panel b. The measured and calculated doses were normalized to the calculated 10 cm depth point along the central axis. Buildup dose at shallow depths were then calculated with Monte Carlo.

The depth dose in the buildup region along the IMRT beam axis was calculated. The percent of dose difference of the two IMRT techniques in the buildup region as a function

of step modulation was measured. Depth dose for individual slabs of solid brass was calculated as a function of brass thickness, field size, and source to surface distance. Energy spectral variation for open and compensated field was calculated. The contaminant dose component in the buildup region was calculated. Buildup dose contributed from photons and electrons that were interacted in MLC were calculated.

5.3.7 Dose in Buildup Versus Source Surface Distance

Dose at 1.0 mm depth with extended SSD was also calculated. This is done to approximate the dose difference with a different SSD which may occur with varying patient treatment techniques and also with different accelerator geometries if a linear accelerator other than a Varian is used. This only approximates the differences one would see with a different accelerator, as a complete simulation of the other accelerator would be required. To approximate the effect due to the modulator to surface distance change, but not SSD change, all the results from both measurements and calculations were corrected using Mayneord's F factor.

5.4 Results

5.4.1 Dose Profile Match at 10 cm Depth

Matched profiles of solid modulator and step and shoot MLC at isocenter depth of 10 cm is shown in Figure 25. Agreement between the measured and calculated profiles was better than ±1.5%.

Monte Carlo versus measured profiles
90 ssd, d10
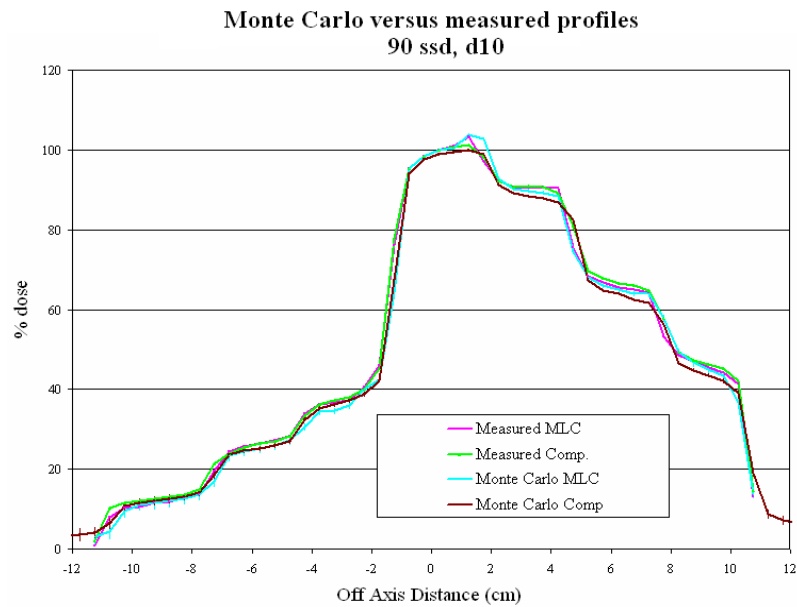
Figure 25.   The matched profiles of IMRT delivery with step and shoot and solid modulator. Center of 6MV beam traverses the thinnest part of the modulator which is 0.6 cm thick brass.

5.4.2 Dose Comparison at Shallow Depths

Agreement between the Monte Carlo and measured data of 3 % or better was achieved for the more clinically relevant IMRT steps of (1, 2 and 3 cm thick) at 1, 3 and 5 mm depth in reference to 10 cm depth, as in Tables 6, 7 and 8.

The measured and calculated dose in cGy (given 100 cGy delivered at isocenter) for the most commonly used clinical compensator with equivalent step thickness of 2 cm, were 47 and 44.0±1.0 for compensator compared to 52 and 49.0±1.5 for MLC at 1 mm depth in Table 6. Table 7 shows the same values for 3 mm depth were 71 and 70.0±1.8 for compensator compared to 75 and 76.0±2.3 for MLC. The same values at 5 mm depth were 83 and 82.0±1.6 for compensator and 90 and 89.0±2.3 for MLC in Table 8. Tables show the same trend of lower compensator dose compared to MLC for more clinically relevant 1 cm and 3 cm thick equivalent steps.

Table 6. Doses (cGy) of IMRT delivery with solid modulator and MLC as a function of STEP thickness of the compensator at 1 mm depth. Doses were calculated with Monte Carlo and measured with parallel plate ionization chamber at 90 SSD, 0.1 cm depth and normalized to dose at isocenter, assuming 100 cGy was delivered at the isocenter.

STEP	COMP		MLC	
cm	Calculated	Measured	Calculated	Measured
0.6	69.0±1.0	69	71.0±1.4	70
1.0	62.0±1.0	64	66.0±2.0	68
2.0	44.0±1.0	47	49.0±1.5	52
3.0	30.0±1.0	30	36.0±1.1	34
4.0	27.0±1.0	29	29.0±1.0	31
5.08	20.0±1.0	21	22.0±1.1	24
7.62	13.0±1.0	12	13.0±1.0	13

Table 7. Doses (cGy) of IMRT delivery with solid modulator and MLC as a function of STEP thickness of the compensator at 3 mm depth. Doses were calculated with Monte Carlo and measured with parallel plate ionization chamber at 90 SSD, 0.3 cm depth and normalized to dose at isocenter, assuming 100 cGy was delivered at the isocenter.

STEP	COMP		MLC	
cm	Calculated	Measured	Calculated	Measured
0.6	113.0±1.7	109	116.0±2.3	113
1.0	100.0±2.0	98	104.0±2.1	102
2.0	70.0±1.8	71	76.0±2.3	75
3.0	50.0±1.5	48	55.0±1.7	53
4.0	39.0±1.2	39	41.0±1.2	43
5.08	27.0±1.1	27	31.0±1.2	31
7.62	15.0±1.0	15	16.0±1.0	15

Table 8. Doses (cGy) of IMRT delivery with solid modulator and MLC as a function of STEP thickness of the compensator at 5 mm depth. Doses were calculated with Monte Carlo and measured with parallel plate ionization chamber at 90 SSD, 0.5 cm depth and normalized to dose at isocenter, assuming 100 cGy was delivered at the isocenter.

STEP	COMP		MLC	
cm	Calculated	Measured	Calculated	Measured
0.6	136.0±2.0	133	138.0±2.8	135
1.0	118.0±1.8	119	123.0±2.8	122
2.0	82.0±1.6	83	89.0±2.3	90
3.0	58.0±1.5	57	62.0±1.9	60
4.0	45.0±1.1	46	47.0±1.6	49
5.08	32.0±1.1	32	34.0±1.4	35
7.62	17.0±1.0	16	17.0±1.0	16

Figure 26 shows percent of dose difference as a function of step modulation for IMRT with MLC versus compensator. The difference increased with compensator thickness reaching the maximum value of 17% for the equivalent of 5 cm thick brass step at 1 mm

92

depth dropping to 8% at 5 mm depth. It decreased with further increase in modulation or

brass thickness, and depth.
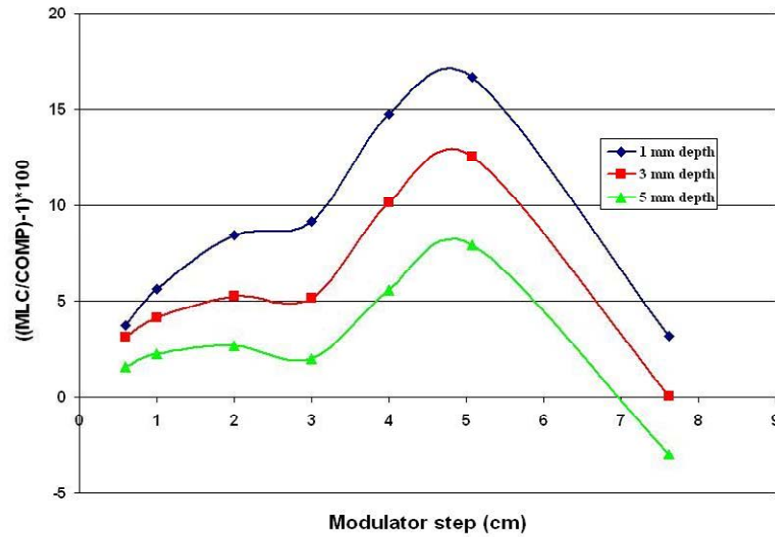
Figure 26. Percent of dose difference for IMRT test delivery with MLC with respect to compensator is shown as a function of step modulation (thickness) for 1, 3 and 5 mm depth. Note the maximum difference occurs for the 5 cm thick step for all depths and is highest for 1 mm depth. The value is about 17%.

5.4.3 Shallow Dose Variation with SSD

Figure 27 shows dose variation with SSD. Dose at 1 mm depth for open beam and beam

attenuated with 1 cm brass was 71 and 64 and did not change with SSD; however. dose

for 5.08 cm brass decreased 10.5% from 56.0 to 45.5 for 90 to 106 cm SSD.

93

5.4.4 Shallow Dose Variation with Field Size

Figure 28 shows dose variation with field size. Dose increased 10 percentage points (67% to 77%) for open beam of (5x5-20x20) cm^2. Dose increase was 12 percentage points (58% to 70%) for 1 cm brass and 25 percentage points (43% to 68%) for 5.08 cm brass.
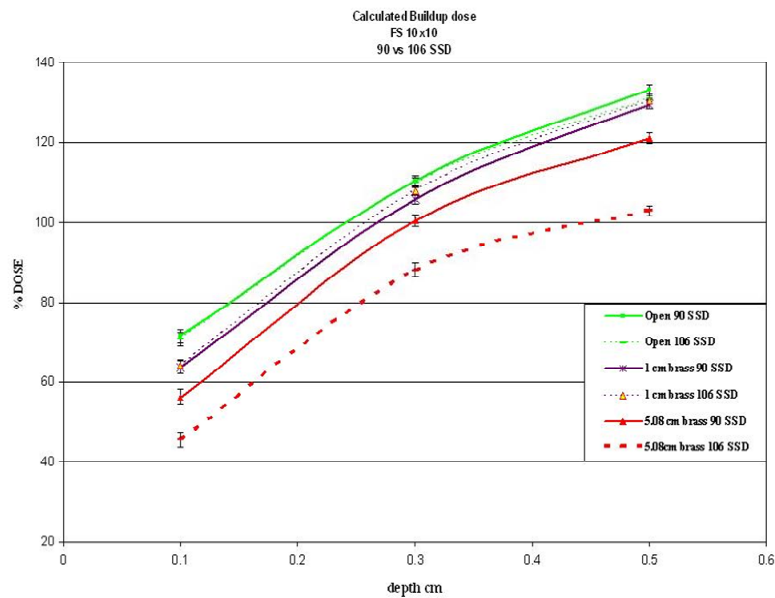
Figure 27. Buildup dose variation with SSD for open and compensated fields. Note the bottom two curves show the largest variation in buildup dose with SSD for the 5.08 cm thick compensator.
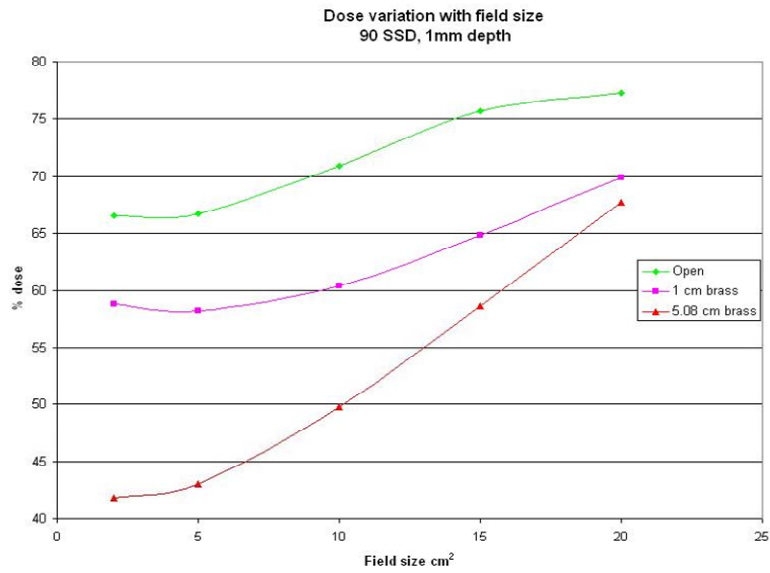
Figure 28. Dose variation with field size. Dose variation for 2, 5, 10, 15 and 20 cm^2 fields is presented for open and compensated fields at 1 mm depth.

5.4.5 Energy Spectra Variation for Open and Compensated Field

The average spectral energy of photons was 1.57 MeV for open beam and 2.17 MeV for 2 cm thick brass, as shown in Figure 29.
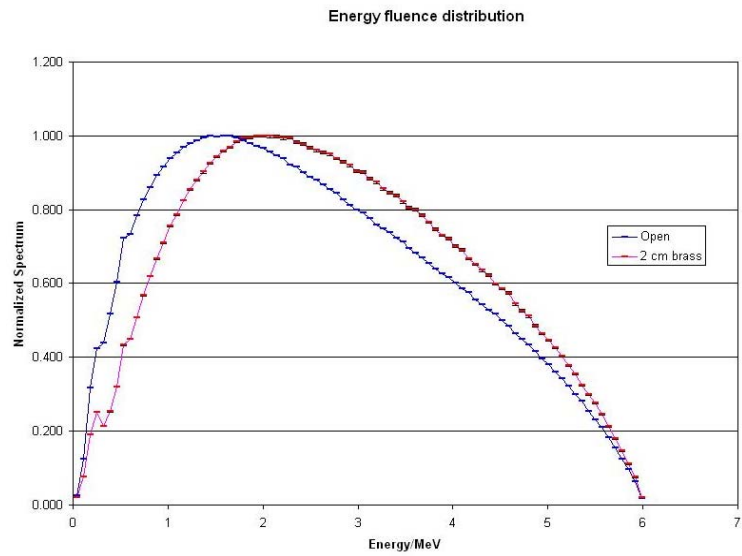
Figure 29. Normalized planar energy fluence distribution of 6MV beam for 2x15 cm^2 field.

5.4.6 Dose Contributions of Various Components

Calculated Component doses of solid modulator and step and shoot MLC as percentage

of total dose is shown in Table 9.

Table 9.   Monte Carlo percent of total dose contribution from scattered photons, contaminant electrons and MLC. Dose at 1.0 mm depth was scored in a 1.5 cm^2 square region centered on the central axis. Set up SSD was (a)=90 cm and (b)=106 cm.

IMRT	Total dose	Scattered Photons	Contaminant Electrons	MLC Component
	cGy	%	%	%
Solid modulator (a)	69.0±1.0	81	19	0.08
Step and shoot (a)	71.0±3.1	82	15	3.0
Solid modulator (b)	50.0±1.0	82	18	0.08
Step and shoot (b)	54.0±2.7	80	18.0	2.0

5.4.7 Scatter Photon Dose Contribution

The primary photons are those generated in the target and pass directly through the flattening filter reaching the phantom surface on the axis with a narrow angular spread and bear minimal scatter component. The contaminant photons or electrons have interacted in and scattered from accelerator head components such as the jaws or MLC before reaching the phantom surface.

These components were differentiated in phantom dose calculation in BEAMnrc. For example, the latch bit filtering in BEAMnrc was used to tag the scattered dose from the MLC. This was accomplished by setting bit 5, for example, in the MLC component module to be associated with this region for use with the bit filters applied when dose components are used. Total dose and dose components were selected for dose calculation in BEAMnrc input file. The particles that were interacted and scattered from MLC entering the phantom were defined to be contaminant. The contaminant type was set to either photon or electron. Finally, the number of dose components inclusive bit filters was defined to include the associated component latch bit filters for component dose calculation.

Low energy scatter photon dose contribution at 1.0 mm depth was 82% of total dose for compensator and 84% of total dose for step and shoot delivery at 90 cm SSD. At 106 cm SSD, these values did not change significantly and were 84% of total dose for compensator and 80% of total dose for step and shoot delivery techniques respectively.

5.4.8 Contaminant Electron Dose Contribution

Contaminant electron dose contribution was significantly lower compared to that from
scattered photons at 1 mm depth. Dose contribution at 90 cm SSD was 18% of total dose
from solid modulator compared to 12% of total dose from step and shoot delivery. The
corresponding values at 106 cm SSD were 16% and 18% of total dose respectively.

Our preliminary calculations in the buildup region at shallower depths near the skin
showed low energy contaminant electrons and photons contributed nearly equally to total
dose. However, the focus of this study was to assess buildup dose between 1-5 mm depth.

5.4.9 MLC Component Dose Contribution

MLC scatter contribution to total dose was less than 0.1% for solid modulator and 2% for
step and shoot delivery. MLC component dose contribution was about 4% of total dose at
shallow depths at 90 cm SSD and 2% at 106 cm SSD respectively.

5.5 Discussion

The results presented here were limited to simple IMRT tests conducted for the step jig
device, however the conclusions that were drawn can be extended to the actual IMRT
plans. The magnitude of this effect is similar to the effect we would expect to see with

large field IMRT plans where the smallest segments are no wider than 2 cm. In cases with much higher degrees of modulation, the MLC scatter would increase.

Usually in treatment planning system calculations, the voxel size is 2-3 mm, and TPS dose calculation uncertainty greatly increases at shallower depths. The dosimetric uncertainty in this region is also pronounced even with Monte Carlo calculations. As the simulation thickness becomes smaller to accommodate calculations at shallower depths, the number of particles interacting in such a thin slab is extremely sparse, hence to perform a calculation with small uncertainty a prohibitively large number of histories would be required to achieve the requisite statistics.

Also, in a separate but related study, Opp et al. analyzed previously planned cases using IMRT with solid compensatrors. In this work, a histogram of transmission factors (plotted by compensator thickness) for 10 cases (with a total of 50 brass modulators) was generated, it is clear that the most probable compensator thickness as weighted by transmission factor (or dose) was just under 2 cm. as shown in Figure 30.
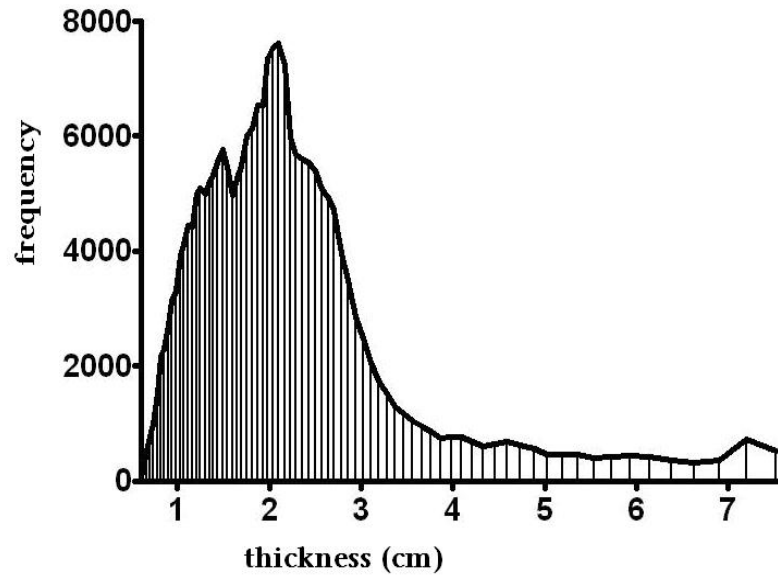
Figure 30. Most probable compensator thickness from 50 retrospective IMRT field analysis (Opp et al.).

The step wedge IMRT simulation calculations for Varian LINAC show dose in the buildup region at depth of 5 mm is 7% lower for compensators with equivalent thickness of 2 cm modulation, compared with MLC. This dose reduction is due to beam hardening of compensators. We conclude that dose at 5 mm depth in the buildup region is 7% lower for compensator- based IMRT compared with MLC-based IMRT delivery on the 6MV Varian Trilogy linear accelerator.

Simulation data indicate dose contribution from MLC at 1 mm depth was less than 3% of total skin dose for step and shoot test delivery. This is partly due to transmission of useful beam through closed MLC leaves (~ 2% for Varian MLC) and partly due to contaminant

radiation emitted from interaction of primary beam with the edges of open MLC segments.

5.5.1 Measured Dose Gradient

Note that making measurements in the buildup region are difficult due to steep dose gradients. The measured dose varied 17%/mm between depth of 2 and 3 mm and 10%/mm between 4 and 5 mm depth.

Acute skin toxicity with step and shoot IMRT for head and neck has been attributed to many factors, including multiple tangential beams, the beam obliquity and the bolus effect of immobilization mask for the head and neck treatments[66]. Authors indicated the average skin dose was 18% larger than the treatment planning system indicated, due to a variety of effects, including the bolusing effect of the mask and beam obliquity.

5.6 Conclusion

Low energy scattered electrons emerging from accelerator head for the step and shoot and brass modulator delivery were major contributors to dose in the buildup region near the surface, which sharply decreased in magnitude while that of photons increased with depth beyond 1 mm, however contaminant contribution from the photons scattered off the MLC increased over the first few millimeters in the buildup region.

The closer the modulator is to the patient, the higher skin dose the patient would get, due to the larger solid angle to the scattered low energy photons and electrons from the accelerator head. In all accelerator configurations, the brass compensator is always closer to the patient than the MLC is. However, Monte Carlo simulations in this study indicate that compensator dose was 5%, 6% and 7% lower than MLC dose at 1 mm, 3 mm and 5 mm depth for modulation equivalent to 2 cm of brass. Beam hardening in the compensator modality is the major reason for its shallow-depth dose sparing in the buildup region. Further extended SSD measurements and simulations in this study suggest that the use of accelerators other than Varian's, which usually have smaller heads, thus larger modulator to surface distance, would further reduce the dose in the buildup region when using compensators.

CHAPTER 6 CONCLUDING REMARKS

The dose in the first few millimieters of the build up region is most strongly influenced by beam spectrum and the SSD. The more the engery spectrum is shifted to higher energy the lower the dose in the buildup region. Similarly the greater the SSD the more the dose in the buildup region is reduced.

In the case of compensators the spectrum is shifted to higher engeries due to beam hardening, and the compensator also filters out the low energy scattered photons and electrons resulting in lower dose in first few millimeters of the the buildup region.

In the case of the Tomotherapy unit the beam has no flattening filter resulting in an energy spectrum that is shifted to lower energies, and the treatments use a smaller SSD. Also the beam angles played a role as beams from shallow angles have longer path lengths.

6.1 Recommendations for Future Work

In radiation oncology there are times when getting a higher dose in the buildup region is desirable, such as in the post-operative setting where cancer cells may have seeded along the surgical scars. In other cases this high dose in the buildup region can cause unwanted

skin reaction and breaks in a patient's treatment. However there is precious little knowledge of exactly what dose to what depth will cause the desired or undesired effects. A clinical investigation may be able to address this issue.

The measurements in the first 4 mm of the buildup region in our work have significant uncertainty. Repeating these measurements with an extrapolation chanber may result in much more accurate measurements which we believe would be in better agreement with our Monte Carlo results.

REFERENCES

1. Leung.Phillip.M.K., Sontag.Marc.R., Maharaj.Harrideo, et al. Dose measurements in the buildup region for Cobalt-60 therapy units. *Med Phys* 1976:3.

2. Taylor.A., Powell.M.E.B. Intensity-modulated radiotherapy-What is it? *Cancer Imaging* 2004; 4(2):68-73.

3. Fraas.B., Doppke.K., Hunt, et al. American Association of Physicists in Medicine Radiation Therapy Committee Task Group 53: Quality assurance for clinical radiotherapy treatment planning. *Med Phys* 1998; 25:1773-1829.

4. Bielajew.A.F., Rogers.D.W.O., Nahum.A.E. Monte Carlo simulation of ion chamber response to 60Co-resolution of anomolies associated with interfaces. *Phys Med Biol* 1985; 30:419-428.

5. Mackie.T.R., Rocwerdt.P.J., Wells.C.M., et al. The OMEGA project: comparison among EGS4 electron beam simulations, 3D Fermi-Eyges calculations, and dose measurements Proc. 11th Int. Conf. on the Use of Computers in Radiation Therapy ed A.R. Hounsell, J.M. Wilkinson and P.C. Williams (Manchester: North Western Medical Physics Department, Christie Hospital NHS Trust). 1994.

6. Mohan.R. Why Monte Carlo? Proc. 12th Int. Conf. on the Use of Computers in Radiation Therapy ed D.D. Leavitt and G. Starkschall (Salt Lake City, UT), Madison, WI:Medical Physics Publishing. 1997:16-18.

7. Kawrakow.I. Accurate condensed history Monte Carlo simulation of electron transport. I. EGSnrc, the new EGS4 version. *Med Phys* 2000; 27:485-498.

8. Kawrakow.I., Rogers.D.W.O. The EGSnrc code system: Monte Carlo simulation of electron and photon transport technical report RIRS-701 (Ottawa, Canada: National Research Council of Canada). 2000.

9. Rogers.D.W.O., Walters.B., Kawrakow.I. BEAMnrc users manual NRC Report PIRS 509(a)revH, (http://irs.inms.nrc.ca/software/beamnrc/). 2004.

10. Ding.G.X. Energy spectra, angular spread, fluence profiles and dose distributions of 6 and 18 MV photon beams: results of Monte Carlo simulations for a Varian 2100EX accelerator *Phys Med Biol* 2002; 47:1025-1046.

11.   Sheikh-Bagheri.D., Rogers.D.W.O. Sensitivity of megavoltage photon beam Monte Carlo simulations to electron beam parameters. *Med Phys* 2002; 29:379-390.

12.   Verhegaegen.F., Seuntjens.V. Monte Carlo modeling of external radiotherapy photon beams. *Phys Med Biol* 2003; 48:R107-R164.

13.   Ma.C.M., Reckwerdt.P., Holmes.M., et al. DOSxyz users manual NRC report. National Research Council of Canada. 1995.

14.   Ma.C.M., Rogers.D.W.O. "BEAMDP Users Manual" National Research Council of Canada Report PIRS-0509D (NRC, Ottawa). 1995.

15.   Javedan.Khosrow, Stevens.Craig.W, Forster.Kenneth.M. Compensator-based intensity-modulated radiation therapy for malignant pleural mesothelioma post extrapleural pneumonectomy. *Journal of Applied Clinical Medical Physics* 2008; 9:98-109.

16.   Aref.A., Thornton.D., Youssef.E., et al. Dosimetric improvements following 3D planning of tangential breast irradiation. *Int J Radiat Oncol Biol Phys* 2000; 48:1569-1574.

17.   Hansen.V.N., Evans.P.M., Shentall.G.S., et al. Dosimetric evaluation of compensation in radiotherapy of the breast: MLC intensity modulation and physical compensators. *Radiother Oncol* 1997; 42:249-256.

18.   Chao.K.S.C., Perez.C.A., Brady.L.W. Breast: locally advanced (T3 and T4), inflammatory, and recurrent tumors. *Radiation oncology management decisions* 2002:367-375.

19.   Hong.L., Alektiar.K., Chui.C., et al. Imrt of large fields: whole-abdomen irradiation. *Int J Radiat Oncol Biol Phys* 2002; 54:278-289.

20.   Ragaz.J., Jackson.S.M., Le.N., et al. Adjuvant radiotherapy and chemotherapy in node-positive premenopausal women with breast cancer. *N Engl J Med* 1997; 337:956-962.

21.   McCormick.B.M., Hudis.C., Dershaw.D.D., et al. Breast cancer, in Principles and practice of gynecologic oncology, edited by W.J. Hoskins, C.A. Perez, R.C. Young, R.R. Barakat and M. Markman. Lippincott Williams & Wilkins, Philadelphia. 2004:1077-1170.

22.   Wells.M., Macmillan.M., Raab.G., et al. Does aqueous or sucralfate cream affect the severity of erythematous radiation skin reactions? A randomised controlled trial. *Radiother Oncol* 2004; 73:153-162.

23. Quach.K.Y., Morales.J., Butson.M.J., et al. Measurement of radiotherapy x-ray skin dose on a chest wall phantom. *Med Phys* 2000; 27:1676-1680.

24. Kron.T., Grigorov.G., Yu.E., et al. Planning evaluation of radiotherapy for complex lung cancer cases using helical tomotherapy. *Phys Med Biol* 2004; 49:3675-3690.

25. Sheng.K, Molley.J.A, Larner.J.M., et al. A dosimetric comparison of non-coplanar IMRT versus Helical TomoTherapy for nasal cavity and paranasal sinus cancer. *Radiother Oncol* 2007; 82:174-178.

26. Cheek.D., Gibbons.J.P., Rosen.I.I., et al. Accuracy of TomoTherapy treatments for superficial target volumes. *Med Phys* 2008; 35:3565-3573.

27. Ramsey.C.R., Seibert.R.M., Robison.B., et al. Helical tomotherapy superficial dose measurements. *Med Phys* 2007; 34:3286-3293.

28. Hardcastle.N., Soisson.E., Metcalfe.P., et al. Dosimetric verification of helical tomotherapy for total scalp irradiation. *Med Phys* 2008; 35:5061-5068.

29. The biological basis for dose limitation in the skin. *ICRU* 1992.

30. Chow.J.C.L., Grigorov.G.N. Surface dosimetry for oblique tangential photon beams: a Monte Carlo simulation study. *Med Phys* 2008; 35:70-76.

31. Lu.W., Olivera.G.H., Chen.M-L., et al. Accurate convolution/superposition for multi-resolution dose calculation using cumulative tabulated kernels. *Phys Med Biol* 2005; 50:655-680.

32. Evans.P.M., Donovan.E.M., Partridge.M., et al. The delivery of intensity modulated radiotherapy to the breast using multiple static fields. *Radiother Oncol* 2000; 57:79-89.

33. Battista.J.J., Sharpe.M.B. True three-dimensional dose computations for megavoltage x-ray therapy: A role for the superposition principle. *Australas Phys Eng Sci Med* 1992; 15:159-178.

34. Rogers.D.W.O., Faddegon.B.A., Ding.G.X., et al. BEAM: A Monte Carlo code to simulate radiotherapy treatment units. *Med Phys* 1995; 22:503-524.

35. Fenwick.J.D., Tome.W.A., Jaradat.H.A., et al. Quality assurance of a helical tomotherapy machine. *Phys Med Biol* 2004; 49:2933-2953.

36.   Tournel.K., Verellen.D., Duchateau, et al. An assessment of the use of skin flashes in helical tomotherapy using phantom and in-vivo dosimetry. *Radiother Oncol* 2007; 84:34-39.

37.   Xiang.H.F., Song.J.S., Chin.D.W.H., et al. Build-up and surface dose measurements on phantom using micro-MOSFET in 6 and 10 MV x-ray beams and comparisons with Monte Carlo calculations. *Med Phys* 2007; 34:1266-1273.

38.   Bang.K.M., Pinheiro.G.A., Wood.J.M., et al. Malignant mesothelioma mortality in the United States, 1999-2001. *Int J Occup Environ Health* 2006; 1:9-15.

39.   Porta.C., Ardizzoni.A., Gaudino.G., et al. Malignant mesothelioma in 2004: how advanced technology and new drugs are changing the perspective of mesothelioma patients. *Med Lav* 2005; 96(4):360-369.

40.   Price.B., Ware.A.. Mesothelioma trends in the United States: an update based on surveillance, epidemiology, and end results program data for 1973 through 2003. *Am J Epidemiol* 2004; 159(2):107-112.

41.   Kutcher.G.J., Kestler.C., Greenblatt.D., et al. Technique for external beam treatment for mesothelioma. *Int J Radiat Oncol Biol Phys* 1987; 13(11):1747-1752.

42.   Soubra.M., Dunscombe.P.B., Hodson.D.I., et al. Physical aspects of external beam radiotherapy for the treatment of malignant pleural mesothelioma. *Int J Radiat Oncol Biol Phys* 1990; 18:1521-1527.

43.   Hilaris.B.S., Non.D., Kwong.E., et al. Pleurectomy and interoperative brachytherapy and post operative radiation in the treatment of malignant pleural mesothelioma. *Int J Radiat Oncol Biol Phys* 1984; 10:325-331.

44.   Bissett.D., Macbeth.F.R., Cram.I., et al. The role of palliative radotherapy in malignant mesothelioma. *Clin Oncol (R Coll Radiol)* 1991; 3(6):315-317.

45.   de.Graaf-Strukowska.L., Van.der.Zee.J., Van.Putten.W., et al. Factors influencing the outcome of radiotherapy in malignant mesothelioma of the pleura - a single-institution experience with 189 patients. *Int J Radiat Oncol Biol Phys* 1999; 43(3):511-516.

46.   Yajnik.S., Rosenzweig.K.E., Mychalczak.B., et al. Hemithorasic radiation after extrapleural pneumonectomy for malignant pleural mesothelioma. *Int J Radiat Oncol Biol Phys* 2003; 56(5):1319-1326.

47.   Meeks.S.L., Buatti.J.M., Bova.F.J., et al. Potential clinical efficacy of intensity-modulated conformal therapy. *Int J Radiat Oncol Biol Phys* 1998; 40:483-495.

48. Ahmad.A., Stevens.Craig.W., Smythe.Roy.W., et al. Promising Early Local Control of Malignant Pleural Mesothelioma Following Postoperative Intensity Modulated Radiation Therapy (IMRT) to the chest. *The cancer journal* 2003; 9.

49. Forster.K.M., Smythe.R.W., Starkshall.G., et al. Intensity-Modulated Radiotherapy Following Extrapleural Pneumonectomy for the Treatment of Malignant Mesothelioma: Clinical Implementation. *1: Int J Radiat Oncol Biol Phys* 2003; 3:606-616.

50. Rice.D.C., Stevens.C.W., Correa.A.M., et al. Outcomes after extrapleural pneumonectomy and intensity-modulated radiation therapy for malignant pleural mesothelioma *Ann Thorac Surg* 2007; 84(5):1685-1692.

51. Malhorta.H.J., Raina.S., Avadhani.J.S., et al. Technical and dosimetric considerations in IMRT treatment planning for large target volumes. *Journal of Applied Clinical Medical Physics* 2005; 6.

52. Chang.S.X., Cullip.T.J., Deschesne.K.M., et al. Intensity modulation delivery techniques: "step and shoot" MLC auto-sequence versus the use of modulator. *Med Phys* 2000; 27:948-959.

53. Chang.S.X., Cullip.T.J., Deschesne.K.M., et al. Compensators: an alternative IMRT delivery technique. *J Appl Clin Med Phys* 2004; 5(3):15-36.

54. DuPlessis.F.C.P., Willemse.C.A. Monte Carlo calculation of effective attenuation coefficients for various compensator materials. *Med Phys* 2003; 30 (9).

55. Jiang.S.B., Ayyangar.K.M.. On compensator design for photon beam intensity-modulated conformal therapy. *Med Phys* 1998; 25 (5).

56. Van't.Reit.A., Mak.A.C., Moerland.M.A., et al. A conformation number to quantify the degree of conformity in Brachytherapy and external beam irradiation: Application to the prostate. *Int J Radiat Oncol Biol Phys* 1997; 37:731-736.

57. Allen.A.M., Xzerminiska.M., Janne.P.A., et al. Fatal pneumonitis associated with intensity-modulated radiation therapy for mesothelioma. *Int J Radiat Oncol Biol Phys* 2006; 65(3):640-645.

58. Slobodan.Devic, Gyorgy.Hegyi, Te.Vuong, et al. Comparative skin dose measurement in the treatment of anal cancer: Conventional versus conformal therapy. *Med Phys* 2004; 31(6):1316-1321.

59. Paelink.L., Wagter.C.D., Esch.A.V., et al. Comparison of buildup dose between Elekta and Varian linear accelerators for high-energy photon beams using radiochromic film and clinical implications for IMRT head and neck treatments. *Phys Med Biol* 2005; 50(3):413-428.

60. Chung.H., Jin.H., Demsey, et al. Evaluation of surface and buildup region dose for intensity-modulated radiation therapy in head and neck cancer. *Med Phys* 2005; 32:2682-2689.

61. Webb.S. The physical basis of IMRT and inverse planning. *The British Journal of Radiology* 2003; 76:678-689.

62. Xing.L., Hamilton.R.J., Spelbring.D., et al. Fast iterative algorithms for three-dimensional inverse treatment planning. *Med Phys* 1998; 25(10):1845-1849.

63. Velkley.D.E., Manson.D.J., Purdy.J.A. Build-up region of Megavoltage radiation sources. *Med Phys* 1975 ;2:14-19.

64. Gerbi.B.J., Khan.F.M. Measurement of dose in the buildup region using fixed-separation plane-parallel ionization chambers. *Med Phys* 1990; 17:17-26.

65. Rawlinson.J.A., Arlen.D., Newcombe.D. Design of parallel-plate ion chambers for buildup measurements in megavoltage photon beams. *Med Phys* 1992; 19:641-648.

66. Lee.N., Chuang.C., Qujyey.J.M., et al. Skin toxicity due to intensity-modulated radiotherapy for head-and-neck carcinoma. *Int J Radiat Oncol Biol Phys* 2002; 53:630-637.

67. Stevens.C.W., Wong.P.F., Rice.D., et al.. Treatment planning system evaluation for mesotheliomaIMRT. *Lung Cancer*. 2005; 49(Suppl 1):S75–S81.

ABOUT THE AUTHOR

Khosrow Javedan lives with his wife Michele Javedan and their son Anthony R. Javedan in Tampa Bay area. He completed his Bachelor's degree at Albion College, Albion Michigan in 1981. He worked at William Beaumont Hospital as an engineer and started his graduate studies in an accredited medical physics program at Wayne State University in Detroit, Michigan and received his Master's degree in medical physics in 1993. He joined Georgetown University hospital working in radiation oncology department as junior physicist and after 2 years as clinical physicist in 1996. He joined Massachussetts General Hospital in 1999 while attending graduate school at University of Lowell. He became board certified in therapeutic medical physics from the American Board of Medical Physics in 1999 and from American Board of Radiology in 2000. He joined the H. Lee Moffitt Cancer Center as a clinical radiation physicist in 2003 and started pursuing his Ph.D. at the University of South Florida in 2004.